Identification and functional characterization of STRN-ALK fusions as a therapeutic target in aggressive forms of thyroid cancer

by

Lindsey Marcell Kelly

Bachelor of Science, Duquesne University, 2005

Submitted to the Graduate Faculty of

School of Medicine in partial fulfillment

of the requirements for the degree of

Doctor of Philosophy

University of Pittsburgh

2015

UNIVERSITY OF PITTSBURGH

School of Medicine

This dissertation was presented

by

Lindsey Marcell Kelly

It was defended on

January 30th, 2015

and approved by

Chairperson: Marie DeFrances, MD, PhD, Associate Professor, Department of Pathology

Daniel Altschuler, PhD, Associate Professor, Department of Pharmacology and Chemical Biology

Urvashi Surti, PhD, Associate Professor, Department of Pathology

Clayton A. Wiley, MD, PhD, Professor, Department of Pathology

Reza Zarnegar, PhD, Professor, Department of Pathology

Thesis Advisor: Yuri Nikiforov, MD, PhD, Professor and Vice Chair, Department of Pathology

Identification and functional characterization of STRN-ALK fusions as a therapeutic target in aggressive forms of thyroid cancer.

Lindsey Marcell Kelly, B.S.

University of Pittsburgh, 2015

Thyroid cancer is a common endocrine malignancy and is currently the fastest growing in incidence in the United States. Thyroid cancers encompass both well-differentiated and dedifferentiated cancer types. Dedifferentiated tumors have high mortality rates and lack effective therapies. Using paired-end whole-transcriptome RNA-sequencing of papillary thyroid cancer, we identified rearrangements involving the anaplastic lymphoma kinase (*ALK*) gene in thyroid cancer. We found that the most common *ALK* fusion in thyroid cancer is between *ALK* and the striatin (*STRN*) gene, which results from the rearrangement of chromosome 2p. *STRN-ALK* fusions did not overlap with other known driver mutations in these tumors, indicating that this rearrangement is a driver event. We found that the dimerization of the STRN-ALK protein by the coiled-coil domain of STRN leads to constitutive activation of ALK kinase. Our results demonstrate that STRN-ALK activation causes ALK kinase-dependent, thyroid-stimulating hormone independent proliferation of thyroid cells. We also show that STRN-ALK expression transforms cells *in vitro* and induces tumor formation in nude mice.

In addition to well-differentiated papillary cancer, we identified *STRN-ALK* with a higher frequency in poorly differentiated and anaplastic thyroid cancers. Dedifferentiation of tumors leads to loss of iodine avidity; therefore, radioiodine treatment of these tumors is no longer an option. ALK fusions are a potential molecular target for treatment of these aggressive tumors. We established that ALK inhibitors crizotinib and TAE684 block STRN-ALK kinase activity

and ALK-kinase induced THS-independent thyroid cell growth *in vitro*. In our preclinical mouse models, growth of tumors from STRN-ALK cells is blocked by crizotinib and LDK378, FDA approved ALK inhibitors. Moreover, LDK378 halts tumor growth of crizotinib resistant STRN-ALK cells. Our data demonstrate that STRN-ALK fusions occur in a subset of patients with highly aggressive types of thyroid cancer and provide evidence that ALK represents a therapeutic target for these patients.

TABLE OF CONTENTS

LIST OF TABLES

LIST OF FIGURES

PREFACE

I would like to thank my advisor, Dr. Yuri Nikiforov, for support he has provided from the time I expressed interest in pursuing my PhD. All the moments where it felt like nothing would ever produce results were met with encouragement. Better yet, the exciting results were met with the appropriate amount of enthusiasm.

I would also like to thank my committee, Drs. Daniel Altschuler, Marie DeFrances, Urvashi Surti, Clayton Wiley, and Reza Zarnegar. I appreciate the time you have spent guiding me through this experience and your suggestions along the way. We collaborated closely with Dr. Altschuler on this project, and I valued his input and the knowledge I gained from our meetings.

There have been many people who have helped me along in this experience that is graduate school, from protocols to reagents to troubleshooting. I would like to thank the members of my lab, Federica Panebianco and Sue Rominski, as well as past members. Also members of Dr. Altschuler's lab. Guillermo Barila really did teach me everything I know about mice, and made an experience that could have been quite dreadful into my favorite part of the project. My friends from my program and labs where I did my rotations have also been quick to help with everything from edits to western blot troubleshooting.

On a personal note, I'd like to thank my parents and their unwavering support, along with my sisters and in-laws. Finally, thank you to my husband for always believing in my abilities and choices, cliché but completely true.

1.0 INTRODUCTION

1.1 THYROID CANCER

Currently, thyroid cancer has the fastest increasing incidence in the United States, and among women is the fifth most common type of cancer [1]. Thyroid carcinoma is a common endocrine malignancy arising from either follicular or parafollicular cells of the thyroid. Only 3-5% of thyroid cancers originate from parafollicular or C-cells, the remaining majority arising from follicular epithelial cells [2]. Our focus is on tumors that arise from follicular cells. Follicular tumors are further divided into benign follicular adenomas, well-differentiated tumors of papillary and follicular carcinoma, poorly differentiated (or insular) carcinoma, and anaplastic (dedifferentiated) carcinoma.

Well-differentiated tumors, papillary thyroid carcinoma (PTC) (80-85% of all thyroid cancer) and follicular carcinoma (FC) (10-15%), are the most common malignant nodules [3]. The follicular variant of papillary thyroid carcinoma (FV-PTC) is a subtype comprising 15% to 20% of PTC. There is no consensus on how many and how prominent the nuclear features should be to consider the neoplasm a FV of PTC. This results in a high interobserver variability reported for classifying challenging cases [4]. Aggressive thyroid tumors can either arise *de novo* or from the stepwise dedifferentiation of FC or PTC and are comprised of poorly differentiated carcinoma (<2% of all thyroid cancer) and anaplastic (undifferentiated) carcinoma (1-2%) [2].

The well-differentiated PTC tumors account for the increase in the number of thyroid cancers reported to the SEER (Surveillance, Epidemiology, and End Results) database (Figure 1); these tumors have nearly tripled since 1975 [3, 5, 6]. The rise in incidence of PTC is partially due to an increase in the diagnosis of the FV-PTC, which grew 3-fold between 1973 and 2003 [7]. Several potential reasons to explain the increased frequency of PTC have been proposed in the literature, such as relaxed histopathologic criteria and advances in thyroid imaging [2, 3, 8]. Thyroid imaging has become more widely available and high-resolution instruments allow for the detection of very small nodules [2]. When the relaxed histopathologic criteria over the last decade is combined with more sensitive detection, it may result in the appearance of an increase in overall frequency.

Several reviews highlighting the increase in incidence in the United States [3] and South Korea [8] have brought attention to the increased screening for nodules and decreasing size of tumors. The authors feel that the increasing incidence of PT is the result of over-diagnosis. They argue that the incidence of dedifferentiated tumors and the rate of death should also have increased if there was a real increase in the number of PTCs.

However, it's difficult to ascertain if the proposed over-diagnosis will account for the entire increase. Chen et al argue that increased sensitivity of detection should result in increased occurrence of only small tumors, but their results demonstrate that though nodules <1cm had the highest rate of increase, all tumor sizes increased [9, 10]. It has also been proposed that exposure to radiation, a known risk factor for thyroid cancer, resulting from more frequent use of medical technology and nuclear power accidents could also be the cause of increased thyroid cancer occurrence [2].

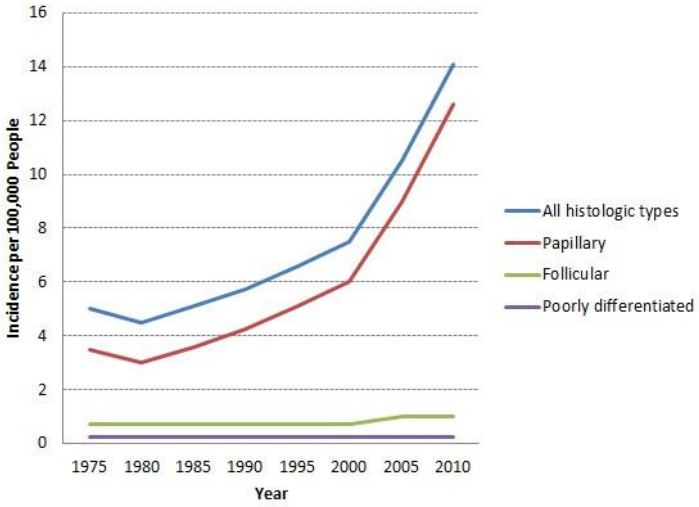

Figure 1: Increasing incidence of thyroid cancer over time as reported to the SEER database

The incidence of thyroid cancer has increased over the last three decades. This rise is due to the increase of papillary thyroid cancer (PTC). The number of follicular thyroid cancers, a well-differentiated tumor, and poorly differentiated tumors has remained relatively constant since 1975. Adapted from [3]

1.2 OVERVIEW OF COMMON MOLECULAR ALTERATIONS IN THYROID CANCER

Mutations in well-differentiated thyroid cancer are almost always mutually exclusive and this suggests that the mutations have similar downstream effects [11, 12]. Indeed, the gene fusions and point mutations in thyroid cancer often involve activation of the MAPK and PI3K-AKT signaling pathways (Figure 2) [2]. These pathways regulate proliferation, differentiation, and survival [2, 11]. Normally, thyroid follicular cell proliferation is controlled by thyroid stimulating hormone (TSH) through the THS receptor (TSHR). Uncontrolled signaling through alternate pathways, namely MAPK, is considered to be crucial for thyroid tumor initiation;

progression and dedifferentiation of thyroid cancer involves mutations that affect PI3K-AKT signaling and other pathways [2, 11].

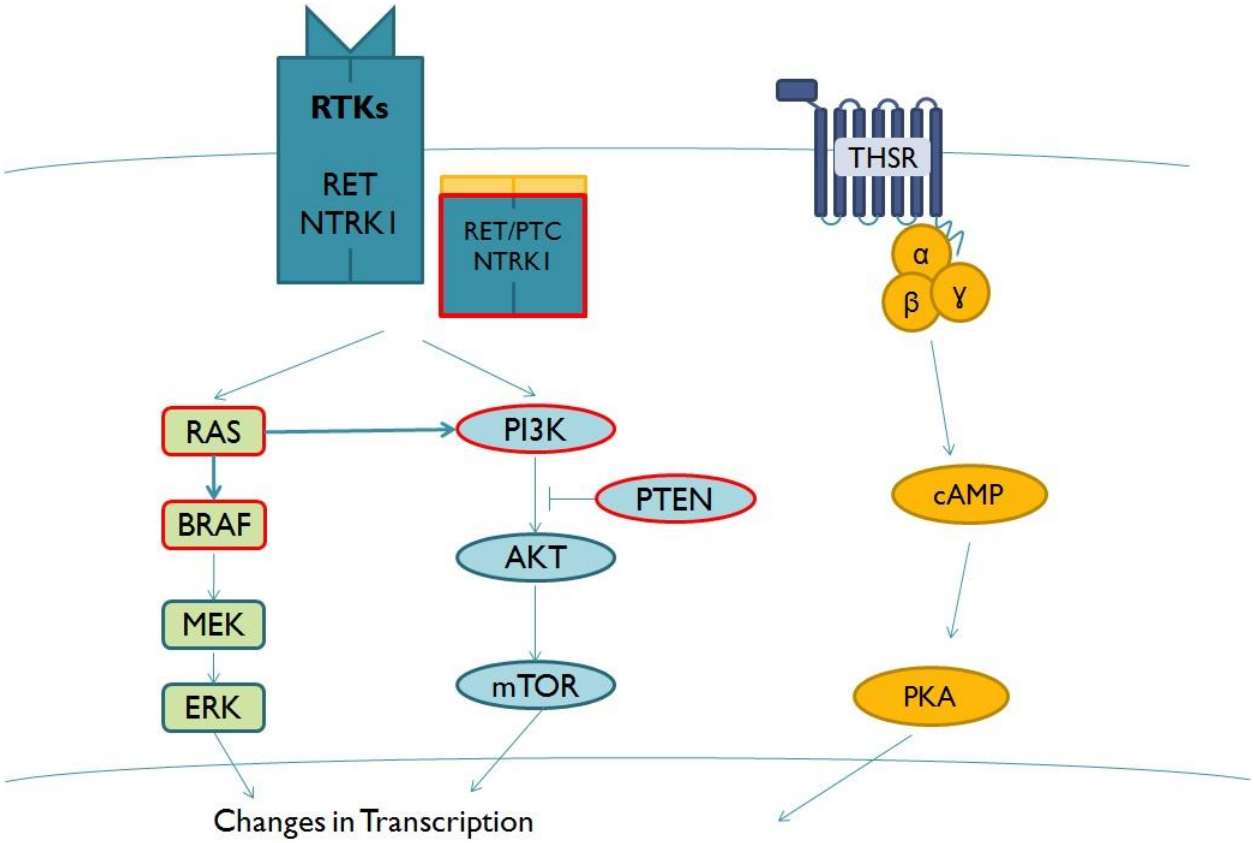

Figure 2: Mutations in thyroid cancer result in the activation of MAPK and PI3K-AKT pathways

MAPK and PI3K-AKT signaling are important to thyroid cancer initiation and progression. Mutations in well-differentiated tumors are highlighted in red and are mutually exclusive, with only rare exceptions. These pathways propagate signals from RTKs through effectors into the nucleus resulting in regulation of cell proliferation, survival, and differentiation. The resulting changes in MAPK and PI3K-AKT pathways bypass the regulation of normal thyroid proliferation controlled by thyroid stimulating hormone (TSH) and the TSH receptor (TSHR).

The common driver mutations, somatic alterations in the cancer genome that are critical to the development of the cancer, in thyroid cancer arise from either point mutations or chromosomal rearrangements. The most frequent mutations found in well differentiated thyroid cancer, activating point mutations in *B-Raf proto-oncogene, serine/threonine kinase* (*BRAF*) and *RAS*, are of the effectors of MAPK and PI3K-AKT signaling. The BRAF T1779A mutation

results in an amino acid change from valine to glutamic acid at position 600, V600E. This mutation disrupts hydrophobic interactions between the G loop and the ATP binding site that normally maintain the inactive conformation leading to constitutively active BRAF kinase activity [13]. *BRAF* mutations in codons 599 and 601 as well as small indels (insertions or deletions) or large scale gene fusions have been reported. *RAS* mutations have also been described and refer to mutations in codons 12, 13, or 61 in *neuroblastoma RAS viral (v-ras) oncogene homolog* (*NRAS*), *Harvey rat sarcoma viral oncogene homolog* (*HRAS*), or *Kirsten rat sarcoma viral oncogene homolog* (*KRAS*) [2].

Chromosomal rearrangements are large-scale genetic aberrations resulting from breakage and improper repair of one or more chromosomes [14]. Rearrangements can affect gene expression in a variety of ways, particularly when the location of the break is within a gene. There is a strong association between chromosomal rearrangements in PTC and exposure to ionizing radiation [14-18]. In post-Chernobyl PTCs point mutations are rare, where as gene fusions that result from chromosomal translocations, such as *RET/PTC*, are found in 50% to 80% of tumors [17]. Other rearrangements such as *A kinase (PRKA) anchor protein 9 (AKAP9*) fused to *BRAF*, *paired box 8* (*PAX8*) fused to *peroxisome proliferator-activated receptor gamma* (*PPARɣ*), and *neurotrophic tyrosine kinase, receptor, type 1* (*NTRK1*) are all more frequent in radiation-associated PTCs but are also present in sporadic thyroid cancers with no reported history of radiation exposure [18, 19].

In the fusion of *PAX8* to *PPARɣ*, the promoter and 5' region of the *PAX8* gene is fused to the entire coding region of *PPARɣ* [20]. PAX8 is a transcription factor highly expressed in thyroid cells and necessary for expression of many thyroid specific genes. PPARɣ is a nuclear receptor transcription factor normally expressed at low levels and with unknown function in the

thyroid [20]. The resulting fusion protein has the DNA binding domains of PAX8 in addition to the normal PPARɣ protein [20]. Although the function is unclear, the fusion protein has been demonstrated to cause abnormal gene expression of both PAX8 and PPARɣ controlled genes [20, 21].

In addition to point mutations, BRAF can also be activated when a gene fusion replaces the N-terminal regulatory regions [11, 19, 22]. The first example of a *BRAF* fusion was found in PTC with the fusion partner *AKAP9*. Exons 1 to 8 in *BRAF* containing the domains that mediate autoinhibition are replaced with exons 1-8 of *AKAP9*. *AKAP9-BRAF* is an oncogene due to the elevated and unregulated BRAF kinase activity of the chimeric protein [19]. *BRAF* fusions with other partners have been detected in PTC and other solid tumors; e.g. *SND1-BRAF*, which was found in three tumors in The Cancer Genome Atlas (TCGA) project and was first reported in a gastric cancer cell line [11, 23].

Receptor tyrosine kinases (RTK) such as *RET* and *NTRK1* are also activated by gene fusions in thyroid cancer. These rearrangements result in the expression of an RTK that is not normally found in thyroid cells. When a gene actively expressed in thyroid cells replaces the promoter and 5' end of the RTK, the newly upstream drives the expression of the RTK, including its kinase domain. The 5' gene also provides the domain for ligand-independent dimerization [24]. For example, *RET/PTC1* is the name for the chimeric mRNA *CCDC6-RET* whose expression is driven by *CCDC6*. In the RET/PTC1 protein the coiled-coil dimerization domain is from *coiled-coil domain containing 6* (*CCDC6*) and the tyrosine kinase domain from *ret proto-oncogene* (*RET*) (Figure 3). It is common for a RTK to have various 5' fusion partners reported. Tropomyosin 3 (*TPM3*), *translocated promoter region, nuclear basket protein* (*TPR*), and *transforming growth factor, beta 1* (*TGF*) all form fusion proteins with *NTRK1* and all result

in the ligand-independent dimerization and activation of the NTRK1 kinase domain [25]. The functional characteristics of chimeric TRK proteins are discussed in further detail below.

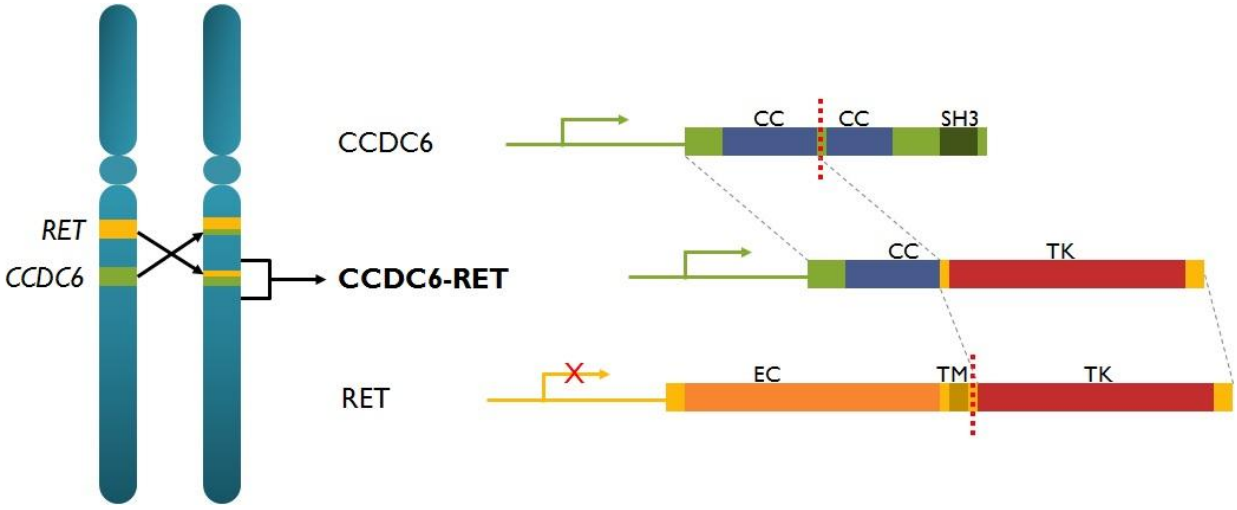

Figure 3: Schematic representation of the *RET/PTC1* gene fusion found in thyroid cancer

RET/PTC1 gene fusion is an example of RTK activation in thyroid cancer. *RET* and *CCDC6* are fused as the result of an intrachromosomal inversion. The *CCDC6-RET* fusion, also known as *RET/PTC1*, places the *RET* tyrosine kinase domain (TK) downstream of the active promoter of *CCDC6* that results in the expression of the chimeric mRNA. The extracellular domain (EC) and transmembrane domain (TM) of *RET* are replaced by and the coiled-coil domain (CC) of *CCDC6*. The second *CCDC6* coiled-coiled domain and Src homology 3 (SH3) are replaced by the TK domain of *RET*.

1.3 FREQUENCY OF SOMATIC MUTATIONS IN WELL-DIFFERENTIATED THYROID CANCER

Papillary thyroid cancers (PTC) most commonly have mutations in *BRAF* (40–45% of cases), and also have mutations in *RAS* (10–20%), *RET/PTC* (10–20%), and *NTRK1* (<5%) [2]. Follicular carcinomas (FC) have mutations in *RAS* (40–50% of cases) followed by *PAX8/PPARγ* (30–35%), *phosphatidylinositol-4,5-bisphosphate 3-kinase, catalytic subunit alpha* (*PIK3CA*)

(<10%), and *phosphatase and tensin homolog* (*PTEN*) (<10%). The higher frequency of RAS and other effectors of the PI3K-AKT pathway indicate that PI3K signaling plays a more significant role in theses tumors compared to MAPK [2]. Mutations are often associated with morphological features. For example *BRAF* mutations are particularly frequent in the tall-cell variant of PTC, where 80% of these histopathological variants are positive [26]. In FV-PTC, *RAS* mutations are the most frequent (35-40% of cases) followed by *BRAF* (25-30%) mutations [2]. Sporadic medullary thyroid cancers that arise from C-cells of the thyroid have *RET* fusions (40-50%) and *RAS* (25%) [2].

1.4 AGGRESSIVE FORMS OF THYROID CANCER

Anaplastic thyroid cancer, ATC, was first described as a rare and highly aggressive malignancy in the 1930s [27]. Poorly differentiated tumors were recognized as a distinct entity much later [28]. The poorly differentiated thyroid carcinoma, PDTC, classification was added by the World Health Organization in 2004, but was more clearly defined by the Turin proposal in 2006 [29]. PDTC represents tumors that are between well differentiated PTC/FC and ATC and is based on discrete biological and clinical criteria [28]. Both ATC and PDTC are thought to arise from a step-wise dedifferentiation of PTC or FC or *de novo* (Figure 4) [28, 30].

1.4.1 Step wise dedifferentiation and *de novo* occurrence of PDTC and ATC

ATC accounts for 1-2% of thyroid cancers, but is found at a higher prevalence, up to 8%, in areas with endemic goiter [28, 31, 32]. The diagnostic criteria of PDTC developed over time,

making the exact incidence of PDTC difficult to determine but it is generally reported to be less than 1% of thyroid tumors [28]. Although PDTC and ATC may form *de novo*, there is evidence that at least some cases occur by dedifferentiation of lesser grade tumors. A history of goiter was reported for ~25% of patients with ATC in a large cohort in the U.S. [33] and has been reported in up to 50% in patient populations from other countries [28, 34, 35]. The same trend was found for PDTC, especially in one population of northern Italy with a high prevalence of goiter; 4-7% of tumors were diagnosed as PDTC in the 1970s-1980s [36, 37]. Also supporting the observation of a link between a history of goiter and ATC, the frequency of ATC dropped in geographic locations of high goiter after iodine supplementation was implemented [28, 38]. However, the mechanism remains unknown. Goiter may predispose to PDTC/ATC due to the higher probability of a well-differentiated tumor from goiter, the increased cell proliferation, or another mechanism [28].

More direct evidence of tumor dedifferentiation is found in tumors that contain areas of ATC adjacent to or within tumors with well-defined features of PTC or FC. In publications that review large series of more than 50 cases, 23-78% of ATCs are thought to have progressed from a PTC or FC [28]. These patients either have a history of a well-differentiated tumor or have areas of well-differentiated tumor co-existing with ATC and more than 80% of the well-differentiated tumors are PTC [5]. These dedifferentiated tumors are highly aggressive. PDTC has a ~50% 10 year survival rate and ATC has a median patient survival of 5 months after diagnosis [30, 39, 40]. While ATC only accounts for <2% of the total number of tumors, it is responsible for 14-39% of all thyroid cancer deaths [33, 41].

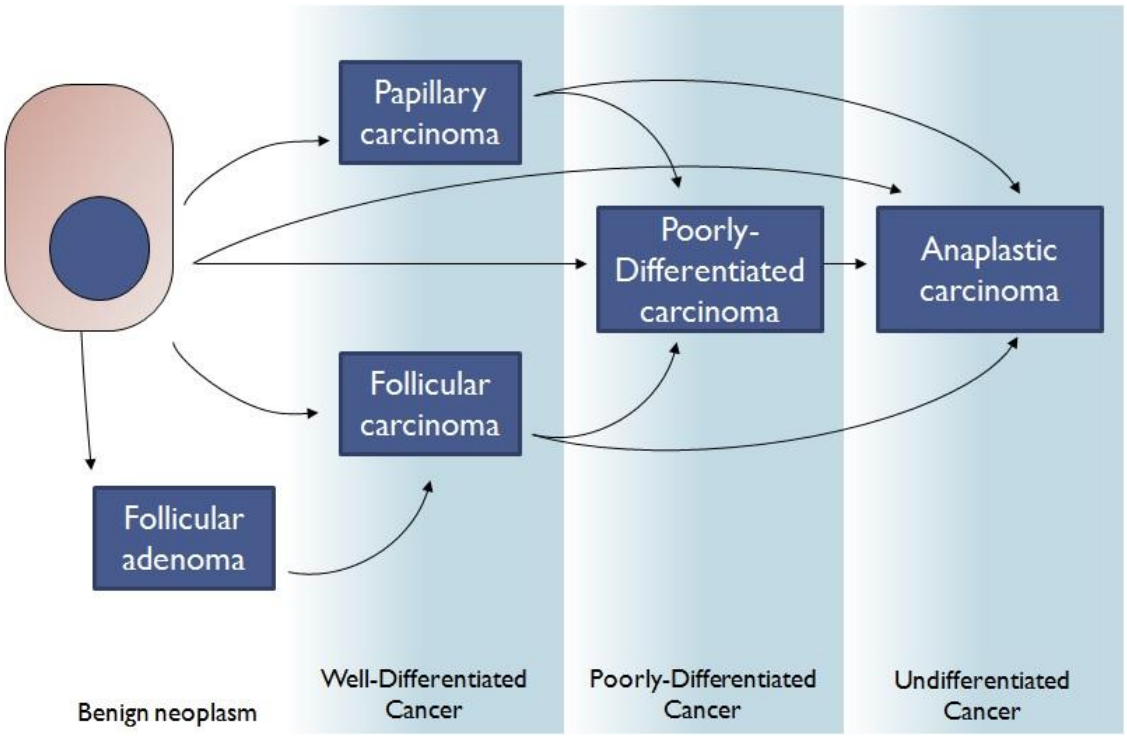

Figure 4: Step-wise dedifferentiation of follicular cells to thyroid cancer.

Follicular cells of the thyroid undergo progression of dedifferentiation to become well-differentiated tumors and then poorly differentiated or anaplastic carcinoma. Although some cases of PDTC or ATC with no history of a lesser lesion, suggesting that they form *de novo*, many patients have a history of goiter or well-differentiated tumor or tumors that retain areas with features of PTC or FC. Adapted from [2].

1.4.2 Frequency of mutations in PDTC and ATC

Well-differentiated tumors characteristically have a single mutation that represents the driver event in the tumor. As tumors dedifferentiate, they acquire additional abnormalities [30]. Somatic mutations found in PDTC and ATC can be divided into two groups that speak to the method of tumorigenesis [28]. The first group of tumors has *RAS* or *BRAF* mutations. PDTC tumors have *BRAF* (15% of cases) or *RAS* (35%) mutations that can also be found in well differentiated areas of the tumor, indicating that the poorly differentiated compartment of the

tumor is arising from these earlier lesions. ATC tumors have similar prevalence of *RAS* mutations, ~30%, and *BRAF* mutations are found in more cases of ATC (~25%) than PDTC [42]. If differentiated areas are present in the ATC, *BRAF* and *RAS* mutations are found in the entire tumor. The presence of mutations in all stages of the tumor suggests that the *BRAF* and *RAS* mutations are early events that predispose the tumors towards accruing more mutations that result in dedifferentiation [28]. *BRAF* mutations have been associated with the reduction of expression of thyroid iodine-handling genes [43] and may be involved in the dedifferentiation [44]. However, *BRAF* alone has not been demonstrated to cause ATC. Although the thyroid-specific mouse model of the *BRAF* V600E mutation generates PTC tumors that progress to dedifferentiated tumors, these tumors do not undergo further transformation to ATC, indicating that BRAF V600E mutations are not able to drive ATC formation [28].

The second group of mutations that occurs in both PDTC and ATC includes *tumor protein p53* (*TP53*) and *catenin (cadherin-associated protein), beta 1, 88kDa* (β-catenin, *CTNNB1*) [28]. *TP53* and β-catenin mutations are rarely found in well-differentiated tumors and only the PDTC or ATC area carries the mutation in tumors with well-differentiated components [28]. This indicates that these mutations are late events in tumor progression. *TP53* mutations are present in 35% of PDTC and are the most frequent mutation in ATC (50-80%) [28, 45, 46]. The sharp increase in prevalence of *TP53* mutations in ATC indicates that this mutation may be crucial to dedifferentiation in thyroid cells [28]. Other mutations are also found in these advanced tumors at lower frequencies including point mutations, i.e. *PTEN* (12%) and *adenomatous polyposis coli* (*APC*) (9%), and chromosomal abnormalities such as copy number gain in *epidermal growth factor receptor* (*EGFR*) and *MET proto-oncogene, receptor tyrosine kinase* (*MET*) [30].

1.4.3 Treatment of PDTC and ATC using targeted therapies

The most common type of thyroid cancer, PTC, has an excellent prognosis with >95% survival rates at 25 years. The standard treatment for PTC is surgery followed by radioactive iodine treatment and TSH suppression [47]. Radioiodine is an effective and specific treatment and can be used to treat tumors that are unresectable or metastatic [47]. The exact mechanism of dedifferentiation of thyroid cancer may be unknown, but it results in the almost universal loss of iodine absorption. Due to this, radioiodine is rarely used for ATC management and there is no standard effective treatment [48]. In addition to radioactive iodine, chemotherapeutic reagents have been unsuccessful. Reports indicate that although there may be a response by the tumor, treatments do not improve length of time from diagnosis to survival or overall survival rates [30].

Mutations and other genetic changes in PDTC and ATC present potential therapeutic targets for patients. Frequently overexpressed in ATC, EGFR has been identified as a therapeutic target [27, 28]. One case study of a patient with ATC showing increased membrane staining of EGFR was treated with erlotinib, a tyrosine kinase inhibitor (TKI), and was reported as having had a favorable response [49]. However, a phase II clinical trial of another EGFR TKI gefitinib included five ATC patients with no response [50]. BRAF is also a potential target; in a phase II study of 20 ATC patients treated with the BRAF inhibitor sorafenib, two (10%) of patients had a partial response and five (20%) had stable disease [51]. Another small study treated a BRAF positive patient with sorafenib. This patient had an increased survival time (19 weeks compared to other non-surgical candidates in the study who had an average survival of 9.1 weeks) [50]. Pazopanib, a multi-targeted VEGF, PDGFR, and c-KIT tyrosine kinase inhibitor, was tested in a phase II trial for metastatic well-differentiated tumors and showed a 49% response rate. However a phase II trial for ATC showed minimal response in 15 patients [50]. These reports suggest that

patients may benefit from targeted therapies. There are still dedifferentiated tumors that no not have mutations identified with available treatments. Identification of novel targets for PDTC and ATC would be very beneficial to these patients.

2.0 IDENTIFICATION OF NOVEL MUTATIONS IN THYROID CANCER USING WHOLE TRANSCRIPTOME SEQUENCING

We used next generation whole-transcriptome sequencing (RNA-Seq) to identify novel mutations in thyroid cancer. In this study we selected aggressive PTC tumors with no known mutations; many of them were FV-PTC. Identifying mutations in these tumors will provide more knowledge about PTC and the FV-PTC tumors that represent the rise in the incidence of thyroid cancer. Beyond increasing our understanding of the pathogenesis of thyroid cancer, discovery of novel mutations provides new therapeutic targets for treatment of aggressive thyroid tumors.

2.1 INTRODUCTION TO RNA-SEQ TECHNOLOGY

RNA-Seq is a high throughput technology that sequences the transcriptome of multiple samples in a massively parallel way. Before next-generation sequencing (NGS) methods were developed, conventional methods such as Sanger sequencing limited the number of sequences that could be generated in a time and cost effective manner. NGS techniques provide quantitative analysis of large regions of the genome with high sensitivity. NGS can be scaled from whole-genome sequencing to targeted multi-gene panels to select the type and amount of information gained for the cost and time available. Whole-transcriptome sequencing (RNA-Seq) has a wide range of applications. This technology can be used to identify the RNA actively expressed in a sample

and provide information about relative levels of gene expression, isoforms present, point mutations, and gene fusions.

RNA-Seq starts with the selection of cases with high quality RNA and then the ribosomal RNA (rRNA) is removed (Figure 5). This purified RNA is converted first into complementary DNA (cDNA) and then to double stranded DNA (dsDNA). The dsDNA is then converted into the "library" for the sample; this refers to the sample's dsDNA that has a small piece DNA ligated onto the end containing the unique sample identifier sequence (barcode) and the sequence captured by the instrument to hold the template during sequencing (adaptor). The library is subjected to testing to determine the quality and exact quantity by several methods. Libraries that pass the quality testing are multiplexed and run on the instrument where the library is sequenced.

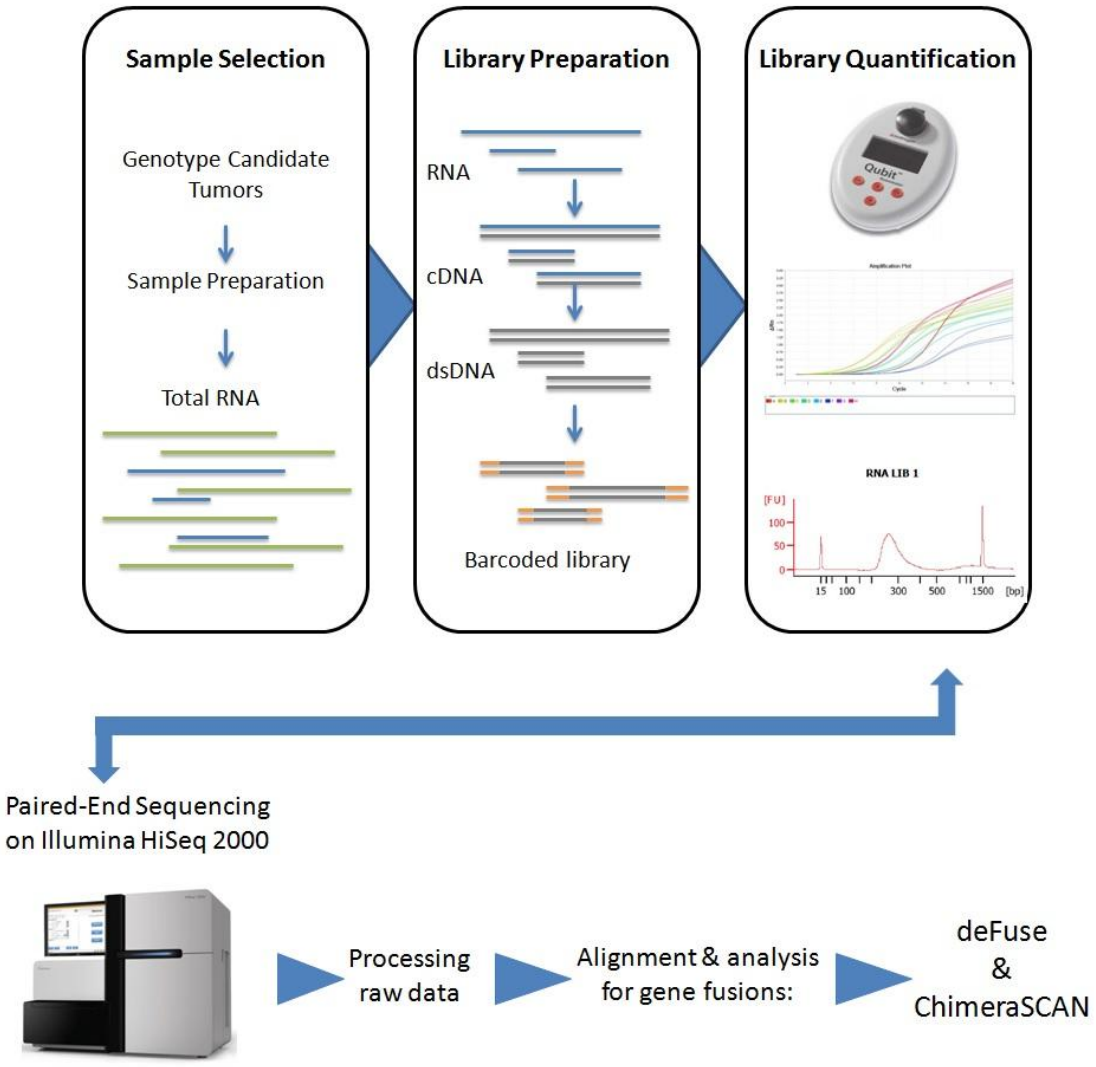

Figure 5: Schematic overview of RNA-Seq procedure

Each individual molecule of the library gets a corresponding sequence that is referred to as a “read” and together are all of the "reads" from the library of each sample. The reads are then subjected to quality control, i.e. filtering out reads that fail due to low base call (quality of each base) or short read length. Then the appropriate program is selected for the data analysis to identify specific information from the reads, such as isoforms expressed or gene fusions present.

Further analysis of the results is often required to select the candidates for validation of the results. We sequenced 21 cases of PTC that were negative for known mutations by RNA-Seq analysis. By sequencing both the tumor and matched normal thyroid tissue, we were able distinguish somatic, tumor specific changes in the transcriptome. This allowed us to identify novel gene fusions expressed in the thyroid cancer.

2.2 SELECTION OF 21 PTC CASES FOR RNA-SEQ FROM 501 CASES

To select cases for RNA-Seq analysis, we started with a pool of 501 consecutive papillary thyroid tumors. Of these tumors, 446 had sufficient material for testing. Tumors were first screened for common mutations such as *RET*/*PTC* and *BRAF*, and then rare mutations that have been reported in the literature to identify candidate cases with no known mutations (Figure 6).

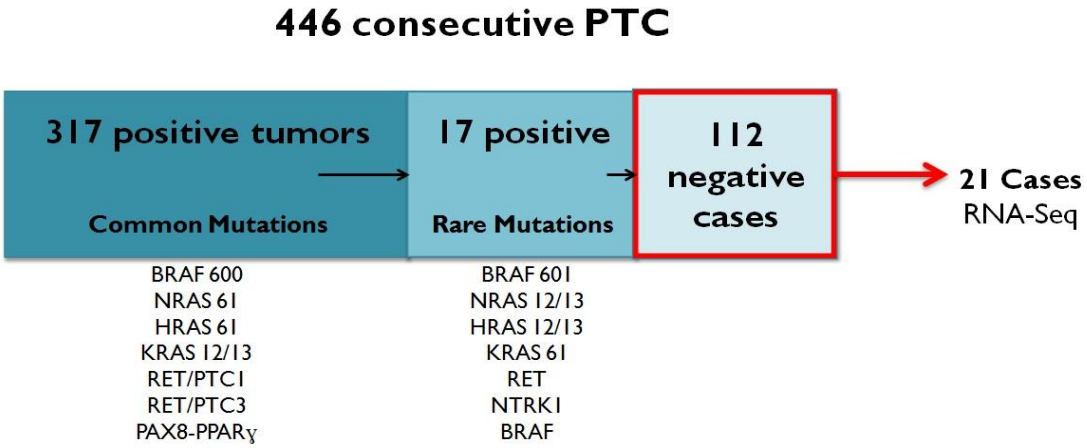

Figure 6: Schematic for the selection of 21 cases for RNA-Seq

In order to select cases with no known mutations for RNA-Seq, 446 cases of PTC were selected for mutational profiling. First the cases were tested for common mutations including *BRAF*, *RAS*, *RET/PTC*, and *PAX8-PPARγ*. The remaining negative cases were tested for rare mutations such as *NTRK1* fusions. From the remaining 129 cases, 21 were selected for RNA-Seq.

2.2.1 Screening 446 PTC cases for common mutations

We used real-time PCR followed by fluorescent melting curve analysis to detect point mutations in *BRAF* codon 600, *NRAS* codon 61, *HRAS* codon 61, and *KRAS* codons 12 and 13. Melting curve analysis is a fluorescent resonance energy transfer (FRET) assay where two probes span the sequence of interest [52]. After completion of the PCR, the products are cooled and the probes anneal to the sequence. The mixture is slowly heated until the probes "melt" off. Probes with a mismatched base will melt at a lower temperature. When the rate of change in fluorescence over time is graphed, peaks are formed for the sequence of template DNA. In other words, each mutation is represented as a peak at a specific temperature different from the wild type peak. The melting curve for each sample was compared to positive and negative control samples to look for unusual melting curve or peaks that deviate from expected temperatures. Sanger sequencing confirmed any case that failed real-time PCR due to late amplification or suspicious melting curve analysis. One example of a rare melting curve identified for BRAF had a mutant peak with a lower than expected temperature (Figure 7A). Upon sequencing, it was determined that this case has a BRAF V600E mutation, but instead of the usual T1799A point mutation, the case had an additional G1800A mutation (Figure 7B). Although the single nucleotide mutations are not common, the resulting amino acid change remained V600E.

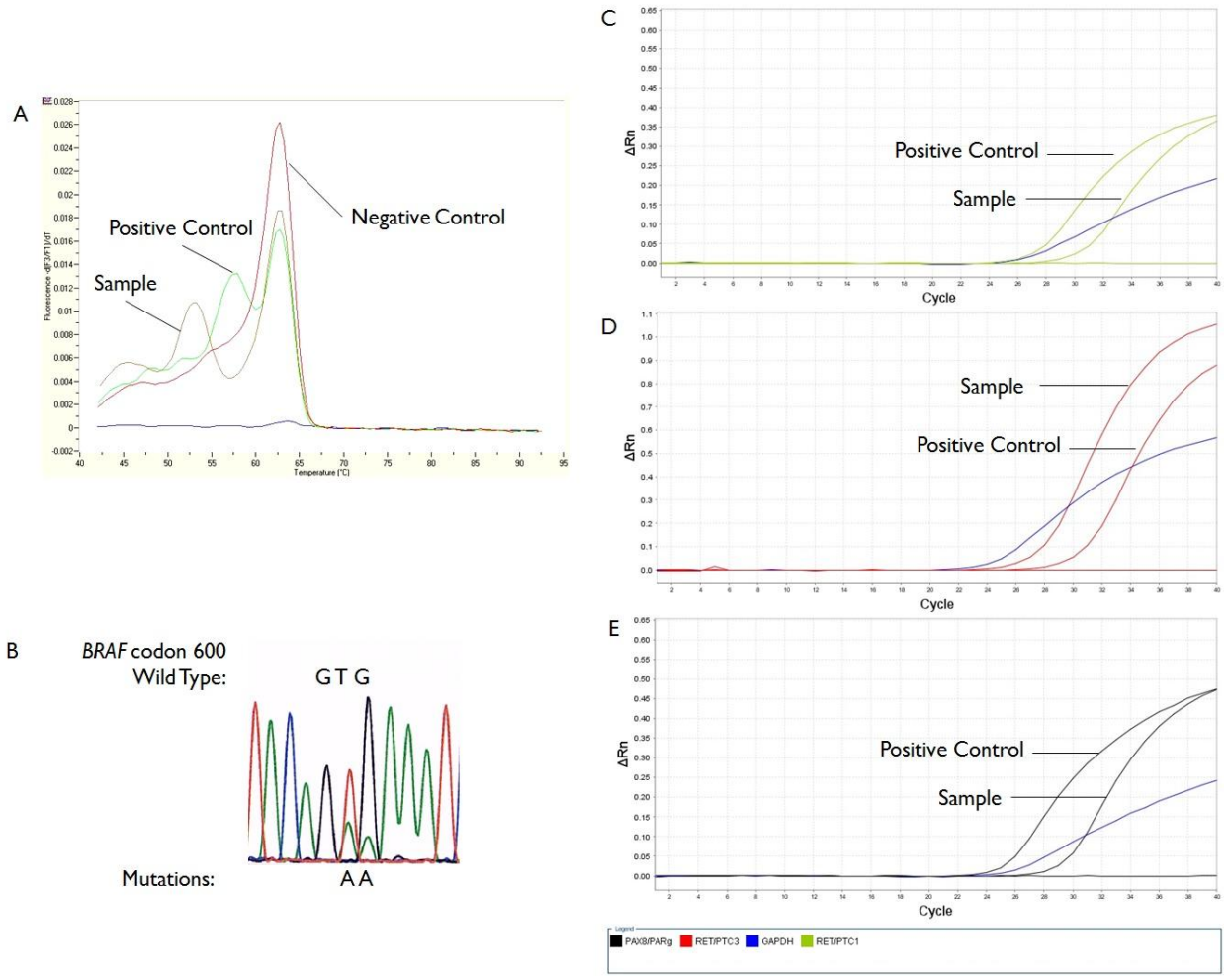

Figure 7: Detection of common point mutations and gene fusions in PTC

A-B, Detection of point mutations using real-time PCR and fluorescent melting curve analysis and Sanger sequencing. (A) Example of an unusual melting curve analysis of *BRAF* real-time PCR. The sample has a low melting temperature peak compared to the positive control (T1799A) sample and the negative control (wild type sequence). (B) Sanger sequencing confirms an additional mutation that still resulted in a V600E mutation. C-D, TaqMan reverse transcription real-time PCR assays with probes covering fusion points. Blue in each plot is GAPDH amplification for the sample. Control GAPDH not shown. (C) *RET/PTC1* positive sample and control. (D) *RET/PTC3* positive sample and control. (E) *PAX8-PPARɣ* positive sample and control.

To test for chromosomal rearrangements that resulted in fusions genes, we selected methods to detect expression of the fusion mRNA. The most common *RET* rearrangements (*RET/PTC1* and *RET/PTC3*) and *PAX8-PPARγ* were detected by TaqMan reverse transcription

real-time PCR assays with probes covering fusion points. These reactions were designed to detect only expressed mRNA and not genomic DNA by using primers that span intron/exon boundaries in addition to the probes that span the fusion point. The TaqMan assays used dual labeled probes that have a fluorescent dye on one end and a nonfluorescent quencher on the opposite end. The quencher blocks the fluorescent signal on the intact probe. The polymerase used had 5' nuclease activity and digests the probe separating the quencher from the dye. The increase in fluorescence from the dye freed from the quencher indicates PCR amplification. Samples that amplified the fusion product below 35 cycles and that also had adequate amplification of the housekeeping gene GAPDH were considered to be positive for the fusion (Figure 7C-D).

In total, we identified 317 (69.5%) tumors were positive for mutations common in PTC including 184 *BRAF* V600E (40.4%), 82 *NRAS* 61 (18%), 33 *HRAS* 61 (7.2%), two *KRAS* 12/13 (0.4%), seven *RET/PTC1* (1.5%), four *RET/PTC3* (0.9%), and five *PAX8-PPARγ* (1.1%) (Table 1). The frequencies of mutations we identified was similar to what is reported in literature, *BRAF* mutations are found in ~40-45% [11, 13, 28]. However there was variability in the less frequent mutations across populations depending on geographic location, radiation exposure, and assay sensitivity [2, 11]. In our sample set, *RET* fusions were found in ~2% of cases but these fusions have been reported to be as high as 20% [28].

Table 1: Prevalence of common mutations in 446 cases of PTC

Mutation	Cases	Percentage, %
BRAF V600E	184	41.3
NRAS 61	82	18.4
HRAS 61	33	7.4
KRAS 12/13	2	0.4
RET/PTC1	7	1.6
RET/PTC3	4	0.9
PAX8/PPARγ	5	1.1
Total Positive	**317**	**71.1**
Negative for mutations	**129**	**28.9**

2.2.2 Screening the remaining 129 cases for rare mutations

In addition to the most common fusions, two other types of *RET* fusions have been identified in thyroid cancer. The first is a *different fusion point* between *RET* with a known fusion partner. The second type is a fusion of *RET* with an *unknown or rare fusion partner*. To detect *NTRK1* and rare fusions of *RET*, we used primers to amplify the kinase domains separately from the extracellular domains using real-time PCR with SYBR green. Since *RET* and *NTRK1* genes are not expressed in follicular cells, any tumor with a high level of kinase domain expression would most likely harbor a gene fusion (Figure 8A). Our group previously identified *AKAP9-BRAF* fusions and we used an RT-PCR reaction designed with primers spanning the fusion point to detect these rearrangements [19]. Sanger sequencing was used to screen additional codons for point mutations in *BRAF* codons 599 and 601, *NRAS* and *HRAS* codons 12 and 13, and *KRAS* codon 61 (Figure 8B-D).

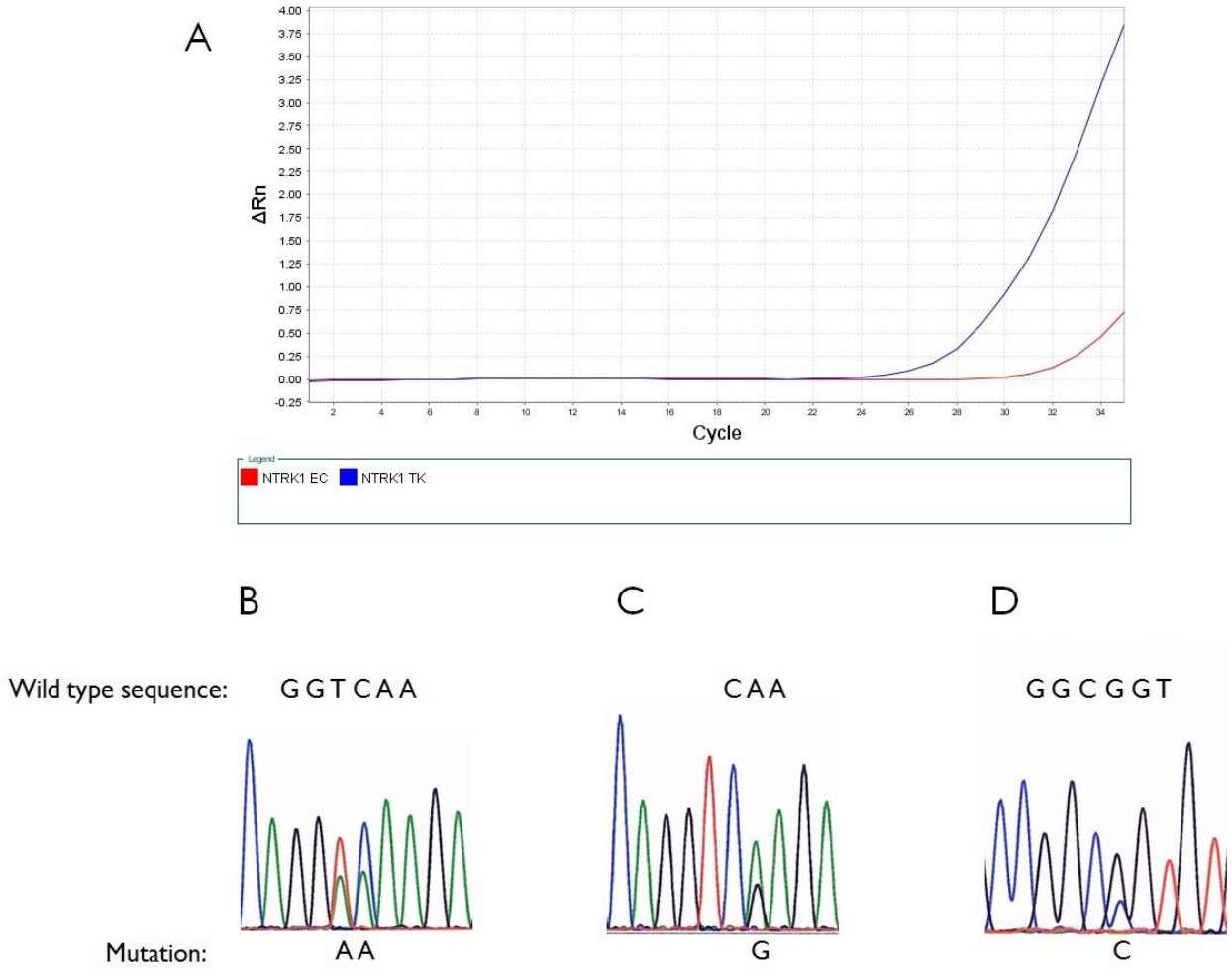

Figure 8: Rare mutations detected in PTC

(A) Detection of increased expression of *NTRK1* tyrosine kinase domain (blue) compared to extracellular domain (red) by real-time PCR with SYBR green. B-D Examples of rare mutations detected by Sanger sequencing (B) *KRAS* G60G and Q61K (C) *KRAS* Q61R and (D) *HRAS* G13R.

The remaining 129 cases were tested for known mutations. This yielded one *BRAF* K601E (0.2%), two *HRAS* (0.4%) and one *NRAS* (0.2%) codon 12 or 13, and seven *KRAS* (1.5%) codon 61 mutations. Five cases were positive for rare fusions, two *RET* (0.4%) and two *NTRK1* (0.4%), and two *AKAP9-BRAF* (0.4%) (Table 2, Figure 9).

Table 2: Prevalence of rare mutations in 446 cases of PTC

Mutation	Cases	Percentage, %
KRAS 61	7	1.6
HRAS 12/13	2	0.4
NRAS 12/13	1	0.2
BRAF K601E	1	0.2
NTRK1	2	0.4
RET	2	0.4
AKAP9 -BRAF	2	0.4
Total Positive	**17**	**3.8**

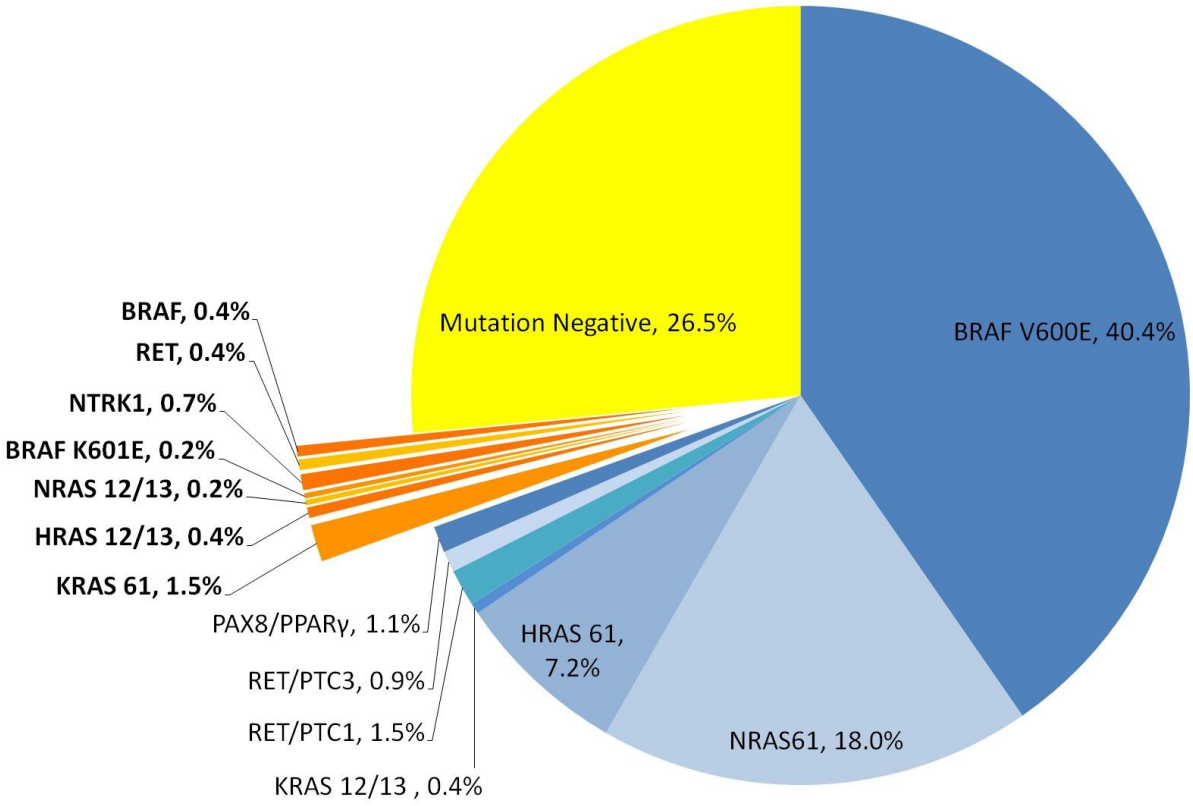

Figure 9: Frequency of common and rare mutations in a series of 446 consecutive PTC cases.

Mutations considered to be common (blue) account for 69.5% of the total cases. Rare mutations (orange) total 3.7%. The remaining cases have no known mutations detected.

2.3 PREPARATION OF RNA-SEQ LIBRARIES FOR 21 CASES

2.3.1 Selection of the cases for RNA-seq from the pool of 112 mutation negative cases

After mutation testing, 112 cases remained negative for known mutations. To select cases for RNA-Seq, we reviewed histology to confirm diagnosis and select cases with aggressive features such as invasion of the capsule. After histological review, we selected cases with adequate tumor and matched normal tissue and isolated RNA. The quality and quantity of the RNA for each sample was precisely measured using the BioAnalyzer (Figure 10). The BioAnalyzer assigns a RNA integrity number (RIN) to samples based on the quality of the ribosomal bands and also the presence of degradation products and other factors [53]. Only cases with normal and tumor tissue yielding RNA with a RIN greater than 6 were accepted for RNAseq.

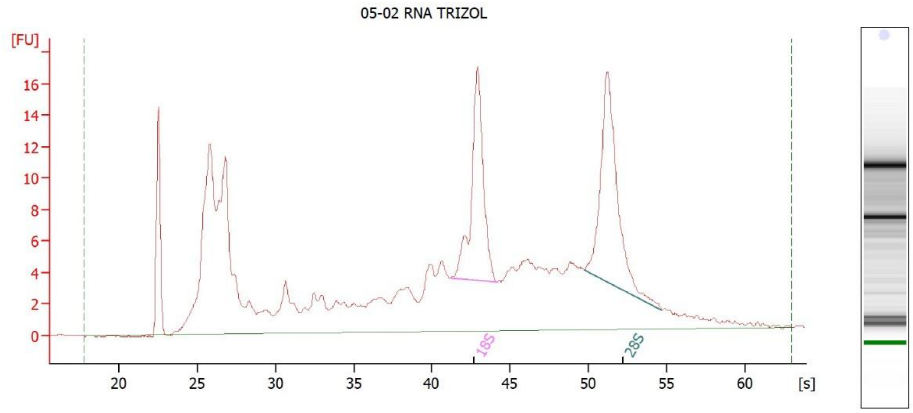

Overall Results for sample 1 : 05-02 RNA TRIZOL

RNA Area:	323.8	RNA Integrity Number (RIN):	7.1 (B.02.08)
RNA Concentration:	249 ng/µl	Result Flagging Color:	
rRNA Ratio [28s / 18s]:	1.2	Result Flagging Label:	RIN: 7.10

Fragment table for sample 1 : 05-02 RNA TRIZOL

Name	Start Time [s]	End Time [s]	Area	% of total Area
18S	41.17	44.18	27.7	8.6
28S	49.70	54.68	32.3	10.0

Figure 10: Representative BioAnalyzer analysis from RNA-Seq sample

BioAnalyzer results for sample 05-02. rRNA is evident as a large proportion of the sample, the RIN, RNA integrity number, for this sample is 7.1 indicating a high quality sample.

2.3.2 Enrichment of the mRNA samples by rRNA removal

The next step in library preparation is to remove the highly abundant rRNA from the sample. There are two strategies to accomplish this; the first is to capture the mRNA by the polyadenylated (poly-A) tail and the second employees probes to target the rRNA sequences for removal. The samples we use for RNA-Seq are clinical samples from patients and although they have been checked for quality, degradation could result in the inability to find fusion products. This is especially critical since many fusion points are far upstream from the poly-A tail. We chose to use an alternative method that targets the rRNA for removal from the sample. The Ribo-Zero Gold kit selectively removes both mitochondrial and cytoplasmic rRNA. This method ensures that the majority mRNA is retained and also presents us with the opportunity to study other RNA species such as ncRNA in future studies.

2.3.3 Preparing the libraries using the Illumina TruSeq RNA Sample Preparation Kit

The pelleted RNA remaining after rRNA removal is added directly to the Illumina TruSeq RNA Sample Preparation kit, which is used to create the library for paired-end sequencing for the Illumina HiSeq2000. As described above, the RNA is converted first to cDNA using a reverse transcriptase reaction. Then the product is cleaned using Agencourt AMPure XP magnetic beads; these beads are used throughout the protocol between each step to capture and retain nucleic acid while remaining reaction components are removed in a series of washes. The next step is to create double stranded DNA (dsDNA) from the cDNA. The dsDNA is cleaned and then used as a substrate for the one-step fragmentation and ligation reaction. In this step, the dsDNA is

randomly cleaved while barcoded adaptors are ligated to the ends of the dsDNA. The library is then cleaned and the quality and quantity is checked.

2.3.4 Determining the concentration and quality of libraries for Paired-End sequencing

In order to attain the maximum amount of high quality sequencing data from the Illumina HiSeq2000, the libraries must be run at concentrations optimized specifically for each instrument. This concentration is determined in using three techniques. First, the concentration and quality are checked using quantitative real-time SYBR green PCR against a standard curve of a control purchased from Illumina with primers specific to the adaptors. Next, the samples are run on the BioAnalyzer, which displays the size distribution of the fragments, the final concentration of the sample as determined by area under the curve, and any contamination that may remain. In the first set of libraries, we detected contamination of Agencourt beads in the libraries run on the bioanalyzer. In subsequent library preparations we added an extended elution to the final step to increase the bead retention by the magnetic separation stand. Finally, the quantity is determined using the Qubit assay for dsDNA that determines the concentration based on dye incorporated into dsDNA but no other nucleic acid. We provided these measurements to the High-Throughput Genome Center at the Department of Pathology, University of Pittsburgh. The samples were run multiplexed; the normal and tumor pair for one patient was run in one lane of the flow cell in the HiSeq2000 instrument. An initial set of six cases was selected as a pilot experiment to ensure that the entire procedure was working correctly before running the remaining cases.

2.4 *ALK* AND OTHER FUSIONS IN PTC IDENTIFIED BY RNA-SEQ

After generating the raw sequencing data, the reads were de-multiplexed by barcode as they were downloaded from the HiSeq2000 instrument. Then the reads were filtered by base quality and length before being analyzed. Two programs, deFuse [54] and ChimeraScan [55, 56], were used to identify gene fusions in our samples. The tumor and its matched normal were analyzed separately and then the fusions detected in the normal were filtered out of the tumor results.

Each program uses a different approach to find gene fusions in paired-end sequencing and provides different output for the fusions detected. The programs varied in basic ways such as the display of the fusion sequence and qualitative metrics for each fusion detected. For example, deFuse provided the predicted consensus sequence of 300-350bp containing the fusion point where as ChimeraScan assigned a unique identifier to each read that spanned the fusion and compiled all reads for a candidate fusion in one excel cell. Although each case also had unique fusions detected by only one program, there were some fusions detected by both programs. We reformatted the data from each program and used UCSC Genome Browser extensively to combine the data sets so that we could characterize each potential fusion mRNA detected.

2.4.1 Pilot study of six PTC cases by RNA-Seq

To ensure that the workflow of procedures from RNA extraction through data analysis returned acceptable results, six cases were selected as a pilot set. One case, 11-14, is presented as an example for the complete analysis process in Tables 3 and 4 and Figures 11 through 13. The reads of the pilot cases were first analyzed using deFuse. Selected data is displayed for chromosome 2 fusions detected in the example case; "splitr_sequence" is the consensus sequence

proposed by deFuse and is truncated for space (Table 3). We selected several candidate fusions for validation by rt-PCR; the candidates included *latent transforming growth factor beta binding protein 1 (LTBP1)* fused to *anaplastic lymphoma receptor tyrosine kinase (ALK)* and another fusion detected by deFuse from the same genomic region *baculoviral IAP repeat containing 6 (BIRC6)* also fused to *LTBP1*. For each fusion, the predicted consensus sequence from deFuse was split into left and right flanking sequences and mapped using UCSC Genome Browser and the BLAT function (Figure 11). The direction of the resulting chimeric mRNAs indicated by arrows pointing from the 5' (left of the fusion point) to the 3' (right) direction of the fusion sequence. We designed primers spanning the fusion point and using rt-PCR, both chimeric mRNA products were detected in the tumor sample but not the matched normal or a *NRAS* positive tumor (Figure 11). An additional 28 cases were tested from the validation set and none were positive. This and other validation data not presented confirmed that the process of isolating RNA, creating and sequencing libraries, and analyzing the data for fusions was successful in detecting gene fusions in the pilot set of cases. We proceeded to sequence the remaining 15 cases.

Table 3: Chromosome 2 results from deFuse analysis for case 11-14

gene_ chromosome1	gene_ chromosome2	cluster_id	gene_name1	gene_name2	splitr_count	span_count	probability	splitr_sequence
2	2	223199	LTBP1	ALK	51	9	0.641381509	GATCAAGTTGCGGCACCTTTTCAGCTGAGTAA
2	2	231487	BIRC6	LTBP1	16	6	0.821471578	GCGGGGGCGGCCGGGGTCTCAGAGTGGCTGC

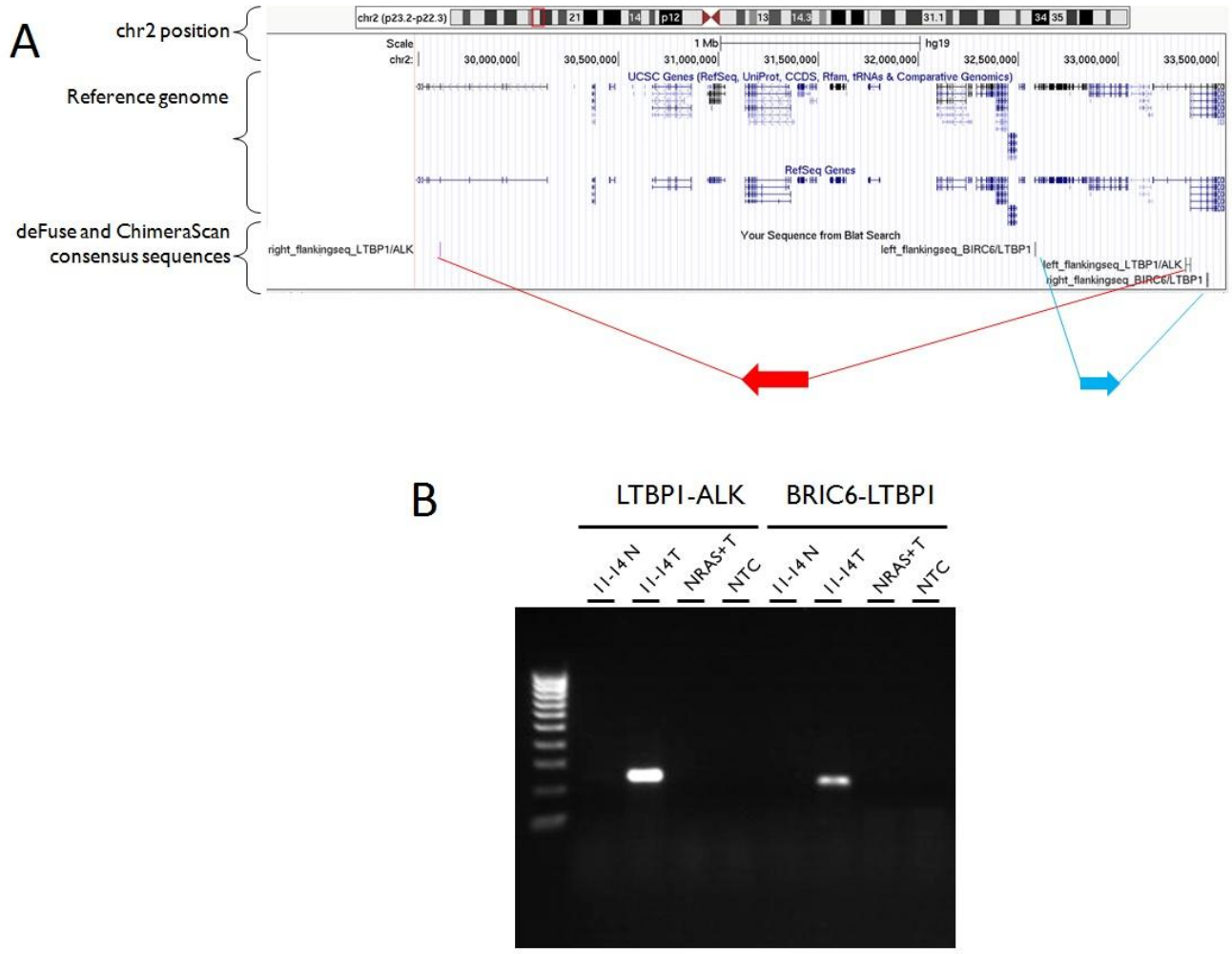

Figure 11: Pilot analysis of the deFuse data for sample 11-14

(A) Analysis of the results from the fusion detection program deFuse using the BLAT tool in UCSC provides a graphical representation to understand the location and orientation of the fusion reads. Two fusions were detected by deFuse involving *LTBP1*, *LTBP1-ALK* represented in red, and *BRIC6-LTBP1* represented in blue. Arrows indicate the 5' (left of the fusion point) to 3' (right) direction of the fusion sequence, also annotated in the sequence name. (B) Validation of the *LTBP1-ALK* and *BRIC6-LTBP1*fusion products by RT-PCR. The normal (N) and tumor (T) samples for the positive case 11-14 were run with tumor that is NRAS codon 61 positive (NRAS+ T) as a control with a no template negative control (NTC). 100bp ladder.

2.4.2 Analysis of RNA-Seq data for 21 cases of PTC

The aim of our study is to identify driver events present in tumor tissue that are not found in normal thyroid tissue. To do this we analyzed all tumors and the matched normal thyroid tissue separately using the deFuse and ChimeraScan programs. The results from each normal tissue sample were filtered out of the results of the corresponding tumor tissue. The remaining fusions detected represent somatic events not present in normal tissue. Overall results the tumors varied from ~11 to 46 fusion events reported per case by the fusion analysis programs. Four tumors were found to have gene fusions, one tumor with a fusion involving *neurotrophic tyrosine kinase, receptor type 3* (*NTRK3*) and three tumors with fusions involving *ALK*.

The *NTRK3* fusion we detected by RNA-Seq was between *NTRK3* on chromosome 15 and the gene *ets variant 6* (*ETV6*) on chromosome 12. The *ETV6-NTRK3* fusion was first described in congenital fibrosarcoma and have been since been identified in several other tumor types, including acute myeloid leukemia (AML), chronic eosinophilic leukemia, congenital mesoblastic nephroma, secretory breast carcinoma, and mammary analog secretory carcinoma of the salivary gland [57-60]. *ETV6* is a member of the ETS transcription factor family, and is involved in other gene fusions resulting from chromosomal translocations that produce oncogenic fusion proteins. The SAM domain of ETV6 is required for the dimerization and activation of the NTRK3 kinase [61].

The *ETV6-NTRK3* fusion was validated using RT-PCR with primers spanning the fusion point between *ETV6* exon 4 and *NTRK3* exon 14. Screening of 151 consecutive PTCs revealed 3 positive tumors, a prevalence of 2%. The *ETV6-NTRK3* mutations were mutually exclusive with other common driver mutations, such as *BRAF* and *RET/PTC*. Analyses of an additional 92

sporadic PTCs were tested from the validation set. This identified 4 tumors that were positive for *ETV6-NTRK3*. Of the seven *ETV6-NTRK3* rearrangements identified in PTCs, six involved the fusion of exon 4 of *ETV6* to exon 14 of *NTRK3*, and one revealed a larger PCR product (Figure 12A). Sanger sequencing of the larger PCR product indicated was caused by the fusion of exon 5 of *ETV6* to exon 14 of *NTRK3* (Figure 12B-D). None of the seven patients who had sporadic PTCs that carried an *ETV6-NTRK3* rearrangement had a documented history of radiation exposure.

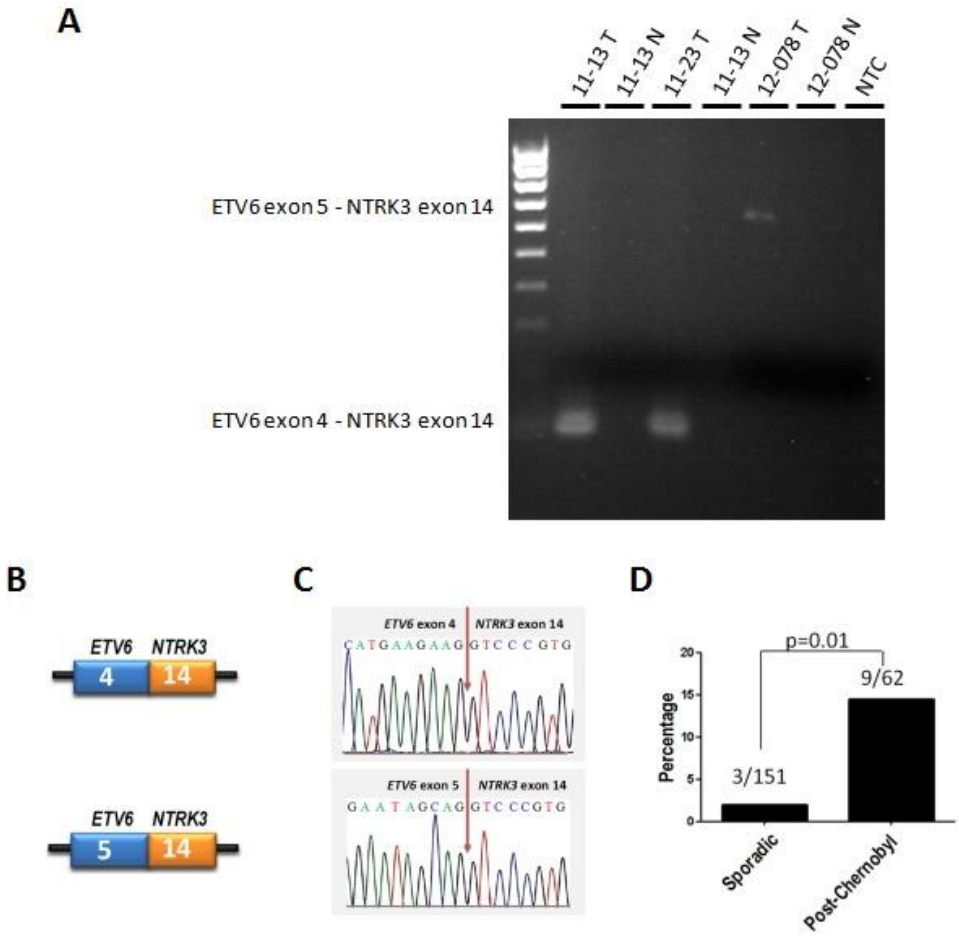

Figure 12: The *ETV6-NTRK3* fusions identified by RNA-Seq

(A) Selected PCR products of the *ETV6-NTRK3* fusion of positive tumors. 11-13T and 11-23T are positive for the exon 4 of *ETV6* to exon 14 of *NTRK3* fusion. 12-078 has a large PCR product that is caused by the fusion of exon 5 of *ETV6* to exon 14 of *NTRK3*. Tumor, T; matched normal, N; with negative control, NTC; and 1kb ladder. (B) Schematic representation of the fusion point between exons of the two genes in mRNA. (C) *ETV6-NTRK3* fusions were confirmed using Sanger sequencing. (D) The frequency of *ETV6-NTRK3* fusions is illustrated in sporadic and post-Chernobyl papillary thyroid carcinomas.

ETV6-NTRK3 fusions reported in various tumor types involve the fusion point initially identified in congenital fibrosarcoma, between exon 5 of *ETV6* and exon 13 of *NTRK3* (31). A

shorter variant, in which exon 4 of *ETV6* is fused to *NTRK3*, has been identified in patients with AML and chronic eosinophilic leukemia [58]. The *ETV6-NTRK3* rearrangements we identified in radiation-related and sporadic PTCs, that differ from those previously identified in other tumor types because they lack exon 13 of *NTRK3*. We published the prevalence of the fusions in sporadic PTC along with the identification of *NTRK3* fusions in radiation associated thyroid cancer, Leeman-Neil and Kelly et al., *ETV6-NTKR3 is a common chromosomal rearrangement in radiation-associated Thyroid Cancer* [16].

3.0 *ALK* FUSIONS IN THYROID CANCER

Using programs designed to detect fusions in RNA-Seq data, we identified two different *ALK* fusions. This is the first report of *ALK* fusions in thyroid cancer. ALK is a member of the insulin receptor protein-tyrosine kinase superfamily. ALK was first identified as an unknown tyrosine kinase in anaplastic large-cell lymphoma and found to be the product of a chromosomal translocation resulting in the fusion protein NPM-ALK [62]. *ALK* fusions have also been described in solid tumors such as non-small cell lung cancer (NSCLC) and inflammatory breast cancer [63]. Although two proteins have been identified as ligands for ALK, other groups have been unable to confirm this; therefore, ALK is considered an orphan receptor tyrosine kinase [64, 65]. ALK is expressed during development and in adult neuronal tissue, but is not known to be expressed in thyroid tissue [65].

In the two tumors identified by RNA-Seq to have *ALK* fusions, exon 3 of *striatin* (*STRN*) was fused to exon 20 of *ALK*. *STRN* is a novel fusion partner for *ALK*. *ALK* and *STRN* are both located on the short arm of chromosome 2 (Figure 13A). *STRN* was first identified in rat brain [66]. Although it has been most commonly studied in neuronal tissue, it is expressed in a wide range of cell lines and tissues including lung, liver, kidney, muscle, placenta, heart, colon, small intestine, and stomach, and is considered to be ubiquitously expressed [67-69]. Wild type STRN binds to caveolin at the cell membrane in a calcium dependent manner [70]. At the cell membrane, STRN and members of the striatin family act as a scaffold to form large multiprotein

complexes that intergrate kinases, phosphatases, and other proteins into the STRIPAK (striatin-interacting phosphatase and kinase) complex [71]. STRIPAK complexes are thought to have cell type specific roles in a diverse range of signaling pathways; however, the function of these complexes remains unknown in most cell types [72]. In endotheial cells, STRIPAK complexes are required for non-genomic estrogen signaling and in neuronal cells the complexes are implicated in cerebral cavernous malformations disease [71, 73]. STRIPAK complexes form using the four protein interaction domains of STRN and other striatin family members: caveolin binding domain (55-63 aa), coiled-coil domain (70-166 aa), calcium-dependent calmodulin-binding domain (149-166 aa), and WD-repeat region (419-780 aa). The coiled-coil domain has been demonstrated to allow STRN to oligomerize [74]; however, one group also found that the caveolin-binding domain was also necessary [72].

The second *ALK* fusion we identified in PTC by RNA-Seq was with *echinoderm mictorubule-associated protein-like 4* (*EML4*). *EML4-ALK* fusions were first described in NSCLC [63] .The fusion detected in our PTC tumor resulted in a chimeric transcript of *EML4* exon 13 to *ALK* exon 20, which is identical to variant 1 in lung cancer. Other variants of *EML4-ALK* fusions have been described with different *EML4* exons fused to exon 20 of *ALK* [75]. Although *EML4-ALK* fusions have been previously reported, this is the first detection of *ALK* fusions in thyroid cancer.

3.1.1 Validation of *STRN-ALK* and *EML4-ALK* detected by RNA-Seq

First we needed to determine that the ALK fusions identified by the RNA-Seq analysis were being expressed in the tumor and not an artifact of library creation or a false positive from alignment in the fusion detection programs. In order to validate the RNA-Seq findings, we

designed primers to flank the fusion points in *STRN*, *EML4*, and *ALK* based on the consensus sequenced identified by deFuse and ChimeraScan. The *STRN-ALK* or *EML4-ALK* fusions were amplified by RT-PCR followed by Sanger sequencing. This confirmed the breakpoints identified by RNA-Seq in all three tumors (Figure 13B, C). We then used a break-apart fluorescent *in situ* hybridization (FISH) probe for *ALK* to confirm the rearrangement at the chromosomal level. In ALK positive tumors, the dual labeled probe shows one yellow signal for intact *ALK* and red and green signals when a chromosomal rearrangement has resulted in the disruption of *ALK* (Figure 13B, C).

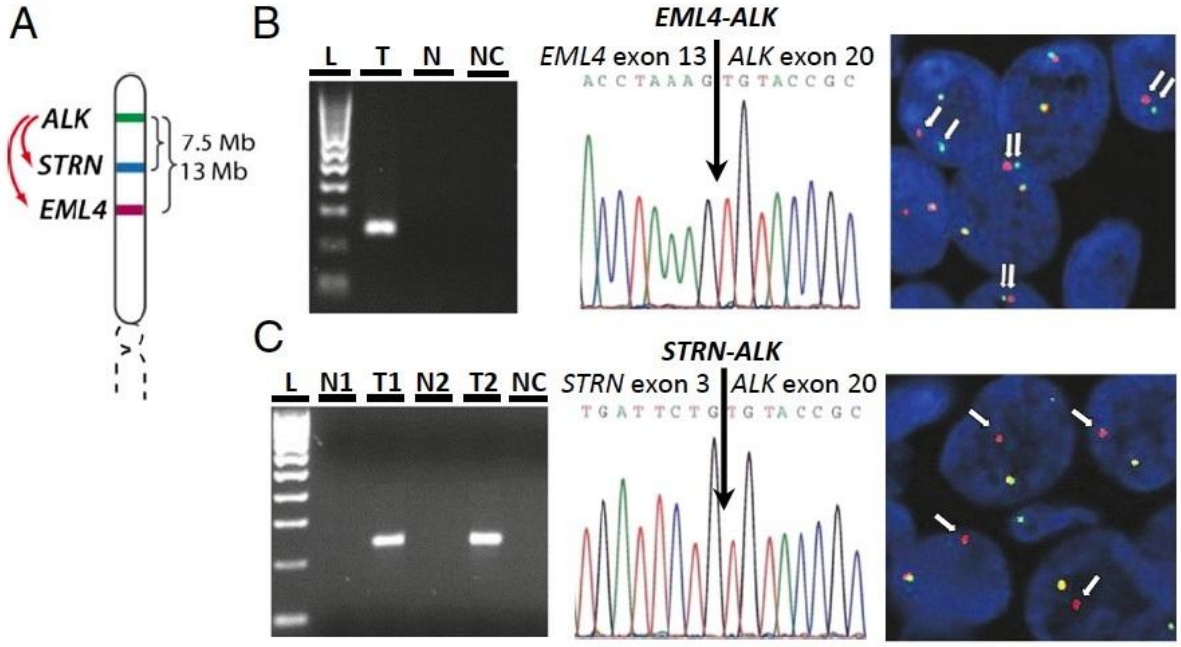

Figure 13: Validation of *ALK* gene fusions detected in thyroid cancer by RNA-Seq

(A) Chromosomal location of *ALK* and its fusion partners, *EML4* and *STRN*, involved in gene rearrangements identified in PTC by RNA-Seq. (B) Confirmation of the *EML4-ALK* fusion by RT-PCR, Sanger sequencing, and FISH with the break-apart *ALK* probe, showing splitting of one pair of red and green signals (arrows). L, 100-bp ladder; N, normal tissue; NC, negative control; T, tumor. (C) Confirmation of the *STRN-ALK* fusion by RT-PCR, Sanger sequencing, and FISH with the break-apart *ALK* probe, showing the loss of green signal in one of the signal pairs (arrows).

Following the validation of the chromosomal rearrangement by FISH, we next identified the genomic fusion point in the intron between STRN exon 3 and ALK exon 20. The breakpoints would be between STRN exons 3 and 4, and ALK exons 19 and 20. We designed an array of primers in the respective gene introns (Figure 14A). We tested the primers in various combinations to identify the general area of the fusion point. Then the specific fusion point between *STRN* and *ALK* in the DNA from both positive tumors was identified using Sanger sequencing (Figure 14B).

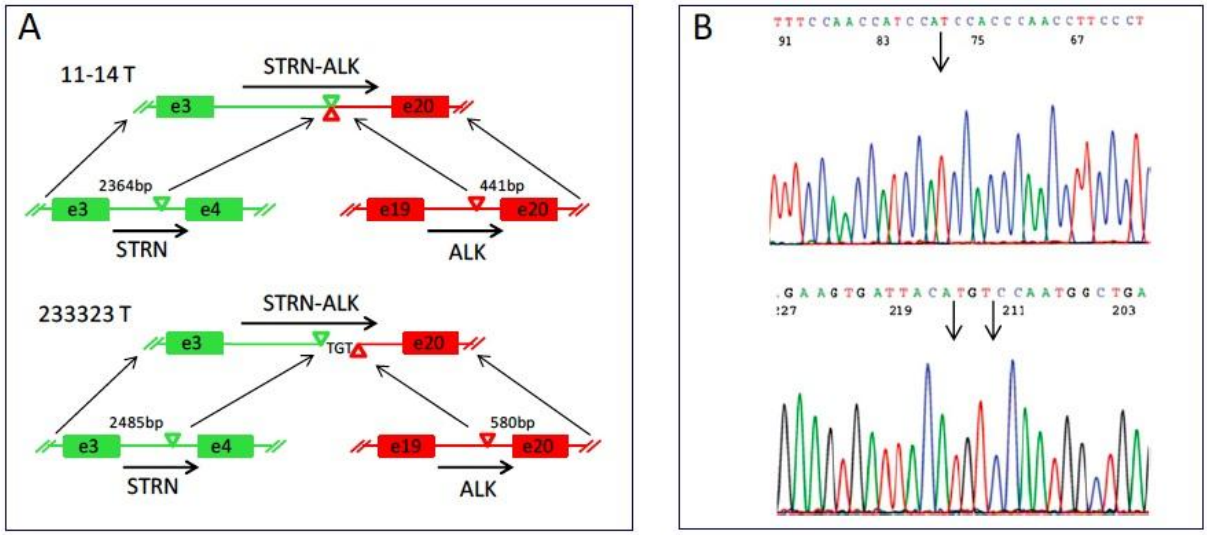

Figure 14: Identification of the genomic position of the STRN-ALK fusions

Using a series of primers designed for regular intervals of the introns between exons 3 and 4 of STRN and exons 19 and 20 of ALK, the fusion point in the genomic DNA of each positive tumor was detected using PCR. (A) A schematic of the fusion points in the introns of STRN and ALK for representative cases. 11-14 T has a direct fusion between STRN and ALK. 233323 T has a three base pair insertion between the fusion point of the introns. (B) Sanger sequencing of the PCR products confirms the fusion between STRN and ALK at the DNA level. The TGT insertion of case 233323 T is present in the sequence.

However, the reciprocal fusion product was not detected by PCR using primers designed after the fusion point was identified. Nor was a reciprocal fusion product detected by RT-PCR or

RNA-Seq. RNA-Seq showed additional fusions involved in region of chromosome 2p surrounding the *STRN* and *ALK* suggesting that there was a complex chromosomal rearrangement resulting in the *STRN-ALK* fusion. The RNA-Seq analysis of tumor 11-14 discussed above revealed *STRN-ALK* and five additional fusion transcripts in chromosome 2 (Tables 3 and 4). When the results from the fusion analysis programs are aligned using BLAT in the UCSC Genome Browser, the fusion products are clustered with in a ~15Mb region (Figure 15). In the process of validation, we confirmed three fusion products as indicated by the arrows. The schematic representation demonstrates the high degree of rearrangement in this area (Figure 16A). Further investigation of this case by FISH using probes for STRN and ALK showed multiple smaller signals for each probe along with the co-localization of the probes indicating the fusion (Figure 16B). Taken together, the RNA-Seq analysis and FISH results demonstrate multiple rearrangements clustered together on a region of chromosome 2p and suggest that chromothripsis [76] may be generating the *STRN-ALK* fusion in thyroid cells.

Table 4: Chromosome 2 results from ChimeraScan analysis for case 11-14

chrom5p	chrom3p	chimera_cluster_id	genes5p	genes3p	total_frags	spanning_frags	score	breakpoint_spanning_reads
chr2	chr2	CLUSTER67	KLHL29	LINC00486	6	1	6	>74924001/1;pos=359;strand=-,CGG
chr2	chr2	CLUSTER585	MRPL33	BRE	2	2	2	>61234490/2;pos=57;strand=+,CAC
chr2	chr2	CLUSTER668	BIRC6	LTBP1	9	8	9	>41698912/2;pos=923;strand=-,GCC
chr2	chr2	CLUSTER515	LINC00486	LTBP1	25	20	25	>93766918/1;pos=514;strand=-,TTC
chr2	chr2	CLUSTER349	LTBP1	ALK	26	24	26	>42297566/1;pos=2113;strand=-,CA
chr2	chr2	CLUSTER721	STRN	ALK	4	4	4	>15035515/2;pos=333;strand=+,CTT

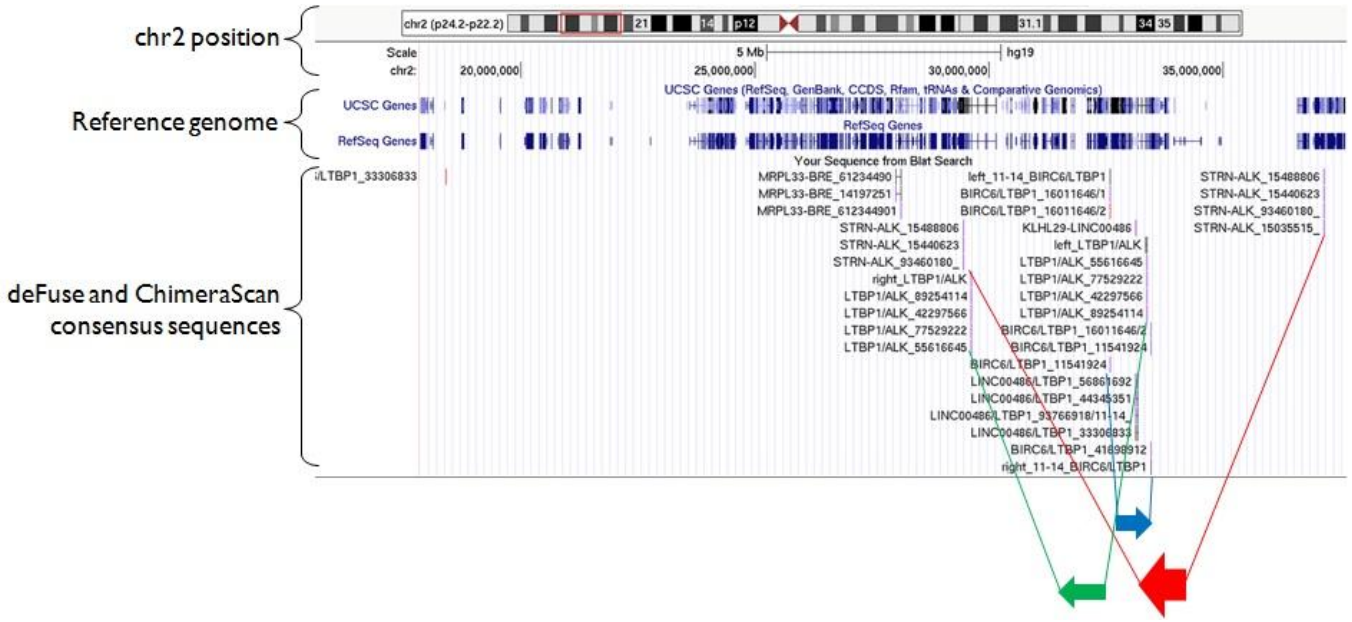

Figure 15: Analysis of deFuse and ChimeraScan results in UCSC Genome Browser

Analysis of the results from the fusion detection programs using the BLAT tool in UCSC Genome Browser provides a graphical representation to understand the location and orientation of the fusion reads. *LTBP1-ALK* represented in green and *BRIC6-LTBP1* represented in blue were detected by deFuse and validated by rt-PCR in the pilot anaylsis. Red arrow indicates the *STRN-ALK* fusion that was detected by ChimeraScan. Arrows indicate the 5' (left of the fusion point) to 3' (right) direction of the fusion sequence. The fusions detected by RNA-Seq are clustered in a region of chromosome 2p with a high level of chromosomal rearrangement.

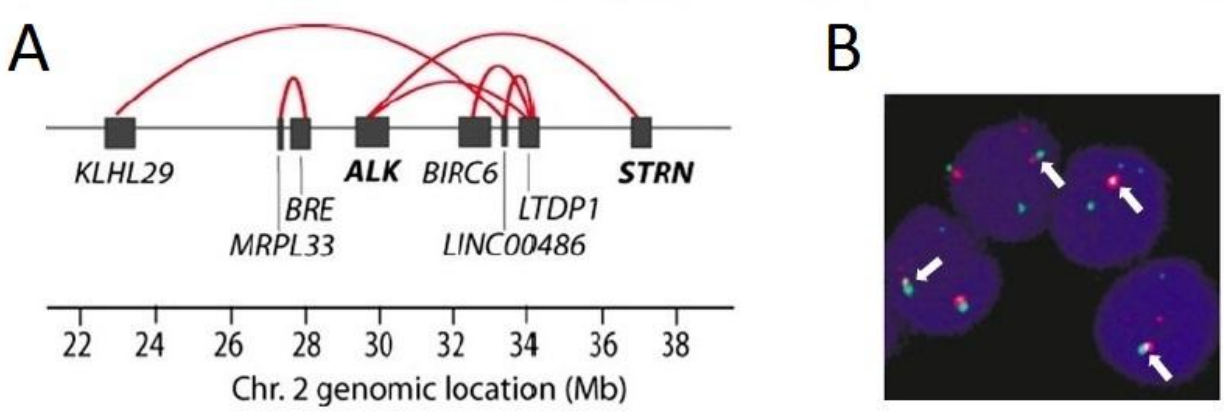

Figure 16: Gene fusions detected by RNA-Seq and FISH in case 11-14

(A) Scheme of gene fusions identified by RNA-Seq in a 15-Mb region of chromosome (Chr.) 2p tumor 11-14 carrying the *STRN-ALK* fusion. (B) FISH with probes for *STRN* (green) and *ALK* (red) showing fusion between the two probes (arrows) and several small fragments of each probe in the tumor cell nuclei, indicating further rearrangements of the part of each probe not involved in the *STRN-ALK* fusion.

3.2 *STRN-ALK* FUSIONS IN THYROID CANCER

3.2.1 The *ALK* tyrosine kinase domain is expressed by *STRN-ALK* fusion

Receptor tyrosine kinases (RTK) such as ALK are frequently activated by gene fusions. The element upstream of the fusion point provides the active promoter to drive expression of the new chimeric mRNA. This mRNA encodes a chimeric protein that contains a dimerization domain fused to the tyrosine kinase (TK) domain of the RTK. As described above, this mechanism is responsible for activating *RET*, *NTRK1*, and *NTRK3* in thyroid cancer after chromosomal rearrangements. The novel fusion of *STRN* to *ALK* results in exons 1-3 of *STRN*,

containing the coiled-coil and caveolin binding domains, fused to exons 20-29 of *ALK* containing the tyrosine kinase domain (Figure 17A). *STRN-ALK* is predicted to result in the expression of the *ALK* TK domain, a kinase that is not normally expressed in thyroid tissue.

The presence of the ALK fusion transcripts was confirmed in the RNA-Seq samples, but the fusion analysis and the validation were not designed to determine the level of fusion expression. To establish the expression of *ALK* in normal thyroid and PTC tissue, we designed primers to separately amplify the extracellular domain and the tyrosine kinase domain of wild type *ALK*. Four normal thyroid tissue samples, three ALK positive tumors, one *NRAS* 61 positive tumor, and five negative tumors were selected. These samples were amplified using quantitative real-time RT-PCR with SYBR green for expression of each *ALK* domain. Analysis of the amplification shows that although wild type *ALK* is expressed in normal thyroid cells at very low levels, thyroid tumors with *STRN-ALK* or *EML4-ALK* fusions express the tyrosine kinase domain an average of 55-fold higher than the extracellular membrane domain of *ALK* (Figure 17C). Other tumors also had very low expression levels, similar to normal thyroid. This demonstrates that *STRN*, the novel upstream fusion partner for *ALK*, is providing the active promoter and driving expression of *ALK* in *STRN-ALK* positive tumors.

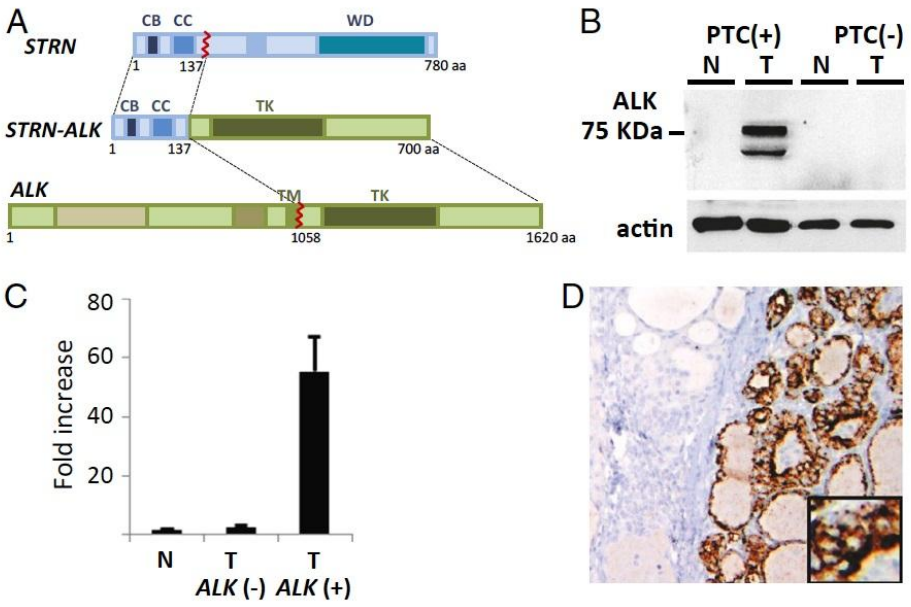

Figure 17: STRN-ALK fusion protein characterization in thyroid tumors

(A) Schematic representation of the fusion of the N-terminal portion of STRN containing the caveolin-binding domain (CB) and coiled-coil domain (CC) to the C-terminal intracellular portion of ALK containing the tyrosine kinase (TK) domain. TM, transmembrane domain; WD, WD-repeat. (B) Western blot analysis of PTC tumors (T) positive and negative for STRN-ALK and corresponding normal tissue (N). (C) Expression level (mean ± SD) of ALK mRNA in normal thyroid cells (N) and tumors negative and positive for ALK fusions detected by quantitative RT-PCR. (D) Immunohistochemistry with ALK antibody to the C terminus showing strong diffuse cytoplasmic immunoreactivity in the tumor positive for STRN-ALK (Right) and no staining in the adjacent normal thyroid tissue (Left). (Magnification: 100×).

3.2.2 Chimeric *STRN-ALK* protein expression in thyroid tumors

The predicted STRN-ALK fusion protein retains the caveolin-binding and coiled-coil domains of STRN, which are fused to the intracellular juxtamembrane region and tyrosine kinase domains of ALK (Figure 17A). The resulting chimeric protein is predicted to be 77kDa in size. We tested a

case positive for STRN-ALK by RNA-seq for the presence of the chimeric protein by western blot analysis using an antibody for the C-terminus of ALK. The western blot showed a band of ~75kDa in the *STRN-ALK* positive tumor (Figure 17B). This confirms the fusion mRNA is producing a protein in tumor tissue. In addition, there was no band in the western blot for wild type ALK at expected molecular weight of 176kDa.

As reported for other ALK fusions, the novel STRN-ALK fusion is between exon 19 and 20 of ALK. The STRN-ALK fusion protein would have loss of the extracellular and transmembrane domains of ALK and is predicted to no longer have membrane anchoring. We preformed immunohistochemistry (IHC) with the ALK antibody to determine the localization of STRN-ALK proteins in fusion positive tumors cells. The IHC staining shows diffuse cytoplasmic localization of the STRN-ALK fusion protein (Figure 17D). The IHC results also confirm the absence of detectable ALK protein expression in normal thyroid cells was shown in western blot. The RT-PCR results of *ALK* extracellular and tyrosine kinase domain mRNA expression, in addition to the western blot and IHC results demonstrate that the novel STRN-ALK fusion detected by RNA-Seq is expressed and translated into protein in thyroid tumor cells.

3.3 CHARACTERIZATION OF THE STRN-ALK PROTEIN

The RT-PCR, western blot, and IHC for the STRN-ALK fusion demonstrate the cytoplasmic overexpression of the ALK tyrosine kinase domain, a kinase that is not normally expressed in thyroid tissue. We next want to demonstrate that STRN-ALK functions as an oncogene in thyroid cancer. To study the function of the STRN-ALK fusion protein, we created a series of HA-epitope tagged constructs and subcloned them into a mammalian expression vector under the

CMV promoter (Figure 18A). The first is a point mutation, STRN-ALK (K230M), in which lysine 230 (Lys1150 in the wild type ALK protein) in the ATP-binding site is substituted by methionine. This mutation has been demonstrated to produce a kinase-dead protein (63). The K230M mutation will allow us to assess the kinase dependent effects of *ALK*. Both the coiled-coil domain and the caveolin-binding domain of STRN have been reported to allow oligomerization of wild type STRN; therefore either could function in allowing the STRN-ALK chimeric protein to dimerize. We created constructs with each of the putative dimerization domains deleted. The caveolin-binding domain of amino acids 54-63 was deleted in STRN-ALK (ΔCB) and the coiled-coil domain of amino acids 70-116 was deleted in STRN-ALK (ΔCC).

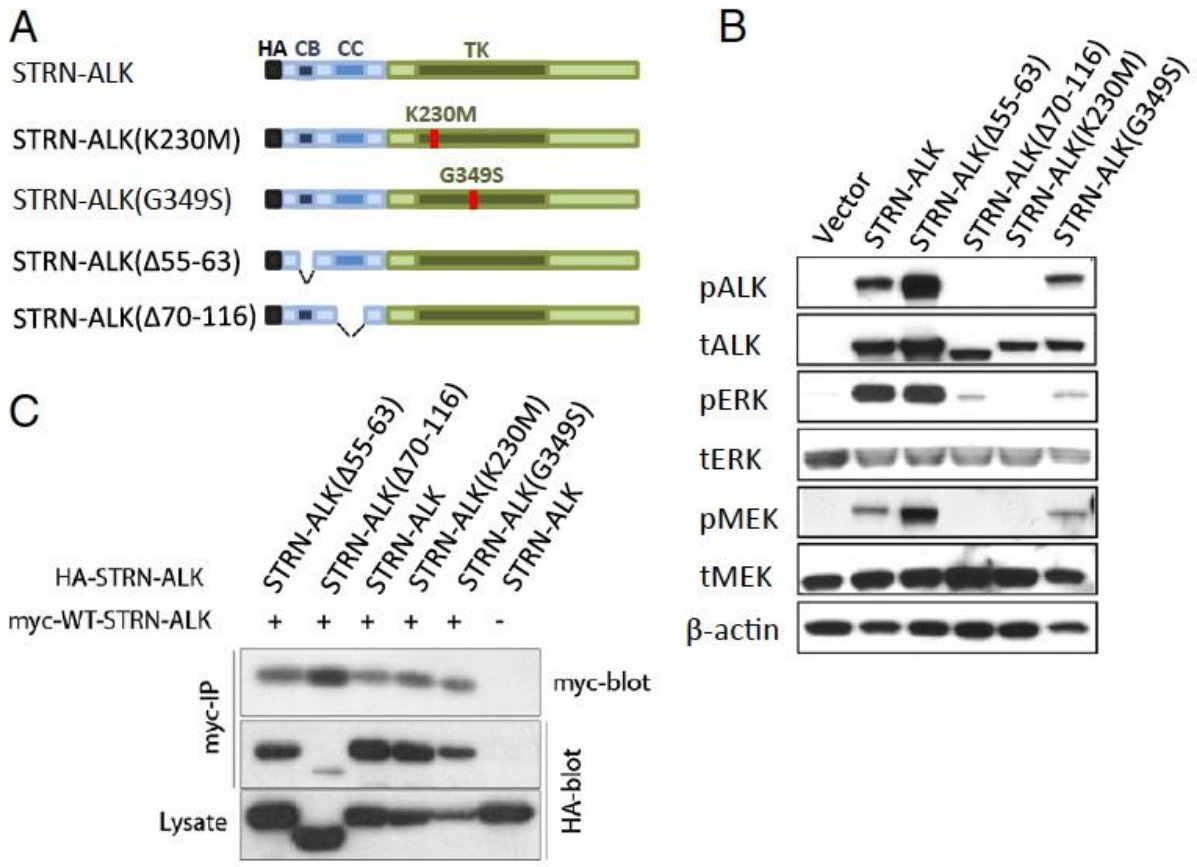

Figure 18: Kinase activity of STRN-ALK requires the coiled-coil domain of STRN for dimerization

(A) Schematic representation of the HA epitope-tagged STRN-ALK construct and its mutants. (B) Western blot of serum-depleted HEK 293 cells transfected with the indicated plasmids showing phosphorylation of ALK (pALK) and induction of pERK and pMEK. tALK, total ALK; tERK, total ERK; tMEK, total MEK. (C) Dimerization assay in HEK 293 cells expressing Myc epitope-tagged STRN-ALK plasmid and one of the HA epitope-tagged plasmids. Cell lysates were immunoprecipitated (IP) with anti-Myc antibody and probed with antibody to HA.

3.3.1 ALK kinase activates the MAPK signaling pathway

MAPK signaling is an essential pathway in PTC (2). ALK fusions in other tumors, as well as RET and NTRK1 fusions in thyroid tumors, activate the MAPK signaling cascade resulting in

cell proliferation (63). To study activation of the fusion ALK kinase domain and associated MAPK signaling, we transfected HEK293 cells with HA-tagged wild type and mutant STRN-ALK. Following transfection, protein lysates were collected and probed via western blot for total (t) and phosphorylated (p) ALK and members of the MAPK signaling pathway ERK and MEK. We used an antibody specific for the phosphorylation of ALK Tyr1278, which correlates with ALK kinase activation [77, 78].

The wild type STRN-ALK fusion led to phosphorylation of ALK, ERK, and MEK (Figure 18B). The kinase dead mutant, STRN-ALK (K230M), had no ALK phosphorylation and did not activate MAPK signaling, indicating that this is an ALK kinase dependent response. Western blot analysis of HEK293 protein lysate after transfection with STRN-ALK domain deletions revealed a difference in ALK activation and signaling. Deletion of the caveolin-binding domain, STRN-ALK (ΔCB), did not affect the phosphorylation of ALK, ERK, or MEK indicating that this domain is not required for kinase activation through dimerization (Figure 18B). However, deletion of the coiled-coil domain, STRN-ALK (ΔCC), resulted in no detectable pALK or pMEK and greatly reduced the level of pERK. These results indicate that tyrosine kinase activity and MAPK signaling by STRN-ALK requires the coiled-coil domain from STRN.

3.3.2 The coiled-coil domain of STRN leads to dimerization of STRN-ALK

Upon ligand binding, most RTKs dimerize to enable autophosphorylation of cytosolic tyrosines leading to activation of the kinase domain [24]. In fusions that result in chimeric RTKs, the N-terminal partner provides the domain for dimerization. In thyroid cancer, the coiled-coil domain of CCDC6, the fusion partner for RET in RET/PTC1, results in the dimerization and activation of RET/PTC1 [79]. The basic domain of EML4 has been shown to mediate EML4-ALK fusion

protein dimerization [63]. As the fusion partner for ALK, STRN is predicted to function by enabling the chimeric protein to dimerize for ligand independent autophosphorylation of ALK.

Both the caveolin-binding and coiled-coil domains have been demonstrated to be necessary for dimerization of wild type STRN [72, 74]. Our western blot results indicated that the caveolin-binding domain is not required for signaling. A co-Immunoprecipitation (IP) assay was used to examine if STRN domains mediate STRN-ALK dimerization. Myc-tagged STRN-ALK was cotransfected into HEK293 cells with HA-tagged STRN-ALK or mutants with deletion of the putative protein interaction domains, STRN-ALK (ΔCB) and STRN-ALK (ΔCC). The lysate from the transfected cells was subjected to Myc-IP and then probed using HA and Myc antibodies. The deletion of the caveolin-binding domain did not affect the amount of HA-tagged STRN-ALK associated with wild type myc-STRN-ALK, indicating that it is not involved in dimerization (Figure 18C). Deletion of the coiled-coil domain greatly reduced the amount of protein pulled down with the wild type Myc-tagged STRN-ALK. These results are consistent with pALK and signaling the data; although there is a faint band present that may indicate that the caveolin-binding domain could possibly have some ability to dimerize *in vitro* there was no pALK protein detected for this mutation to suggest ALK kinase activity. We have demonstrated that the coiled-coil domain from the novel N-terminal fusion partner STRN allows the STRN-ALK protein to dimerize and provides a mechanism for ALK phosphorylation and MAPK signaling.

3.3.3 STRN-ALK increases proliferation and transforms thyroid cells

After establishing the dimerization and activation of the ALK kinase and the associated MAPK signaling, we studied the ability of STRN-ALK to function as an oncogene in thyroid cells. The

PCCL3 rat thyroid epithelial cell line was selected as normal thyroid model. Unlike many human thyroid cell lines, PCCL3 cells are dependent on thyroid stimulating hormone (TSH) for growth in culture [80, 81]. Additionally, they possess many characteristics of differentiated thyroid cells; PCCL3 cells trap iodine and express thyroglobulin, thyroid peroxidase and the TSH receptor [80]. Due to these features, PCCL3 cells are considered to be the closest model of normal thyroid cells *in vitro* and were used to examine if the ALK kinase activity of STRN-ALK fusions affects the proliferation and transformation of thyroid cells.

PCCL3 cells were transfected with STRN-ALK or kinase dead STRN-ALK (K230M) and deprived of TSH. IF staining for HA revealed that cells expressing STRN-ALK with active kinase had a spindle-shape and bifringent appearance (Figure 19A). This change in cell shape is associated with a transformed-like phenotype [81]. Kinase dead STRN-ALK (K230M) expressing cells retained a normal appearance. BrdU assay was used to calculate cell proliferation in PCCL3 cells that expressed STRN-ALK. Cells that expressed kinase active STRN-ALK showed increased TSH-independent cell proliferation that was dependent on ALK kinase activity (Figure 19B). These results indicate that the kinase activity of STRN-ALK increases cell proliferation and transforms the cells in a TSH-independent manner.

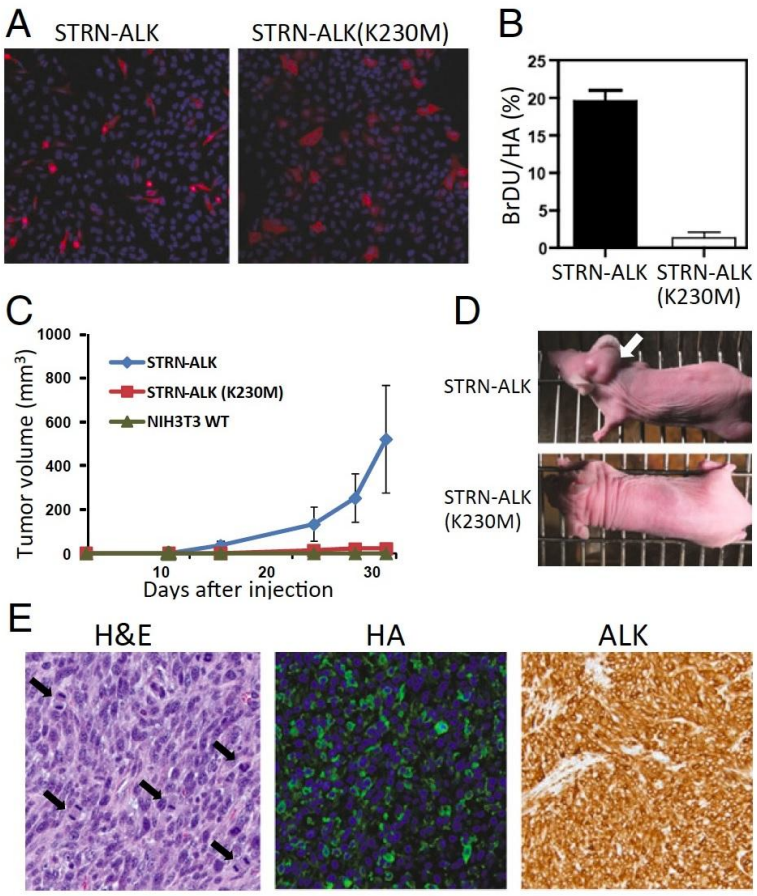

Figure 19: STRN-ALK increases proliferation and induces cell transformation and tumor formation.

PCCL3 cells transfected with HA-STRN-ALK and kinase dead HA-STRN-ALK (K230M) showed cytosolic expression of the introduced protein on HA immunofluorescence and the kinase-dependent transformed like phenotype seen as spindle-shaped and birefringent cells (A) and kinase dependent proliferative response as assessed by BrdU labeling (B). (C–E) Transformation and tumorigenic properties of NIH 3T3 cells transfected with STRN-ALK and kinase-dead STRN-ALK (K230M). (C) Kinetics of tumor growth in xenografts of NIH 3T3 cells in nude mice injected s.c. in the neck with 1×10^7 cells expressing STRN-ALK, kinase-dead STRN-ALK (K230M), or nontransfected NIH 3T3 cells. (D) Representative mice showing tumor formation (arrow) at the site of injections of cells expressing STRN-ALK and no tumor formation at the site of injection of kinase-dead STRN-ALK (K230M). (E, Left) Microscopic appearance of tumors formed at the site of inoculation showing sheets of spindle cells with five or more mitoses (arrows) seen per one high-power field. H&E stain. The tumor cells express the HA-STRN-ALK construct as seen by immunofluorescence with anti-HA antibody (Center) and immunohistochemistry with anti-ALK antibody (Right). (Magnification: 200×).

3.3.4 STRN-ALK drives tumor formation in nude mice

Subcutaneous xenograft tumor formation in immunodeficient mice is commonly used to show the ability of a candidate gene to be tumorigenic [82]. To assay the tumorigenicity of STRN-ALK, we transfected NIH 3T3 cells and subcutaneously injected $1x10^7$ cells into the neck of nude mice. STRN-ALK cells developed tumors in seven of eight mice and the tumors were recognizable after 13 days (Figure 19C, D). Kinase dead STRN-ALK (K230M) and untransfected NIH 3T3 cells did not form discernible tumors (n=8 mice for each group). Analysis of the STRN-ALK tumors by H&E stain showed features of aggressive tumors including high mitotic activity (Figure 19E) and focal tumor necrosis. IF using HA antibody and IHC for ALK confirm the tumors express the HA-STRN-ALK construct. Our results demonstrate that STRN-ALK has the ability to generate xenograft tumors in an ALK kinase dependent manner.

3.4 SUMMARY OF THE CHARACTERIZATION OF THE NOVEL STRN-ALK GENE FUSION

Using RNA-seq we identified *STRN-ALK* and *EML4-ALK* fusions in thyroid cancer. We validated these fusions using RT-PCR for mRNA expression followed by Sanger sequencing, which confirmed transcript detected by the deFuse and ChimeraScan analysis programs. The fusion was also detected in genomic DNA using FISH to demonstrate chromosomal rearrangement and PCR followed by Sanger sequencing to identify the genomic position of the fusion in the intron between STRN and ALK.

The fusion results in the expression of a protein we detected by using a C-terminal ALK antibody of ~75kDa, the predicted size of the STRN-ALK fusion protein. Gene fusions involving RTKs in thyroid cancer result in the upstream partner, providing an active promoter and driving the expression of the downstream gene, in this case the novel partner *STRN* is leading to the expression of *ALK* and its kinase domain. We demonstrate that *STRN* drives the expression of the *ALK* kinase domain 55-fold higher than expression in normal and ALK negative tumors and confirmed that *ALK* is not normally expressed in thyroid tissue at levels detected by western blot.

Consistent with ALK fusion oncogenes detected in other tumor types, our results indicate that STRN facilitates the dimerization of ALK leading to autophosphorylation and signaling of MAPK pathway. Although some data published for wild type STRN suggests that the caveolin-binding domain is required for dimerization [72, 74], we demonstrate that only the coiled-coil domain of STRN is required for dimerization, activation of ALK, and downstream signaling. The dimerization and activation of STRN-ALK performs as an oncogene, increasing cell proliferation and transforming thyroid cells. MAPK activation is essential for tumor initiation in thyroid cells [2, 11], and the activation of this pathway by STRN-ALK supports the evidence that STRN-ALK is an oncogene in PTC.

3.5 PREVALANCE OF ALK FUSIONS IN THYROID CANCER AND ASSOCIATION WITH AGGRESSIVE DISEASE

We identified two *STRN-ALK* and one *EML4-ALK* fusion in our pool of 21 cases for RNA-Seq. This set represented a group of PTC tumors selected for their characteristics of aggressive phenotypes, such as capsule invasion or extrathyroidal extension. As discussed above, mutations

in thyroid cancer can help to determine the malignancy of the tumor; *BRAF* mutations are associated with more aggressive PTCs [2]. Mutations in tumors are also indicative of their progression from lesser lesions. In well-differentiated tumors with areas of ATC or PDTC, *TP53* mutations are found only in the dedifferentiated components of the tumor and are associated with the process of dedifferentiation [28]. To understand how ALK fusions contribute to thyroid cancer and progression we needed to determine the prevalence of the mutations in tumors across all stages.

We used the primers designed for validation of the RNA-Seq cases by RT-PCR to detect *STRN-ALK* expression in the tumors. The specific *EML4-ALK* fusion detected by RNA-Seq was identical to variant 1 detected in NSCLC. There are 4 common variants of *EML4-ALK*, variants 1, 2, 3a, and 3b. The 3a and 3b versions differ by a small inclusion of 33bp [75] and can be detected using the same forward primer. We designed a multiplexed reaction with three *EML4* forward primers paired with a reverse primer for *ALK* to test for the three most common *EML4-ALK* fusions in one reaction. The cDNA for each sample was also tested for expression of GAPDH to indicate adequate RNA quality and successful cDNA synthesis.

First additional PTC and other well-differentiated tumors, follicular carcinoma and medullary carcinoma, were screened. RT-PCR for *EML4-ALK* and *STRN-ALK* fusions revealed one further tumor positive for *STRN-ALK* in 235 cases of PTC. No additional *EML4-ALK* positive tumors were detected. There were no fusions in 36 follicular thyroid carcinomas and 22 medullary carcinomas. In total, we identified three *STRN-ALK* and one *EML4-ALK* positive tumors in 256 samples of PTC resulting in an overall frequency of 1.6%. This places *ALK* fusions at approximately the same frequency as *RET* fusions, *RET-PTC1* 1.5% and *RET-PTC3* 0.9% of tumors were positive in the series of tumors studied.

Next we focused on dedifferentiated tumors and tested PDTC and ATC for expression of *STRN-ALK* and *EML4-ALK* fusions. *STRN-ALK* was identified in three of 35 (9%) PDTC and one of 24 (4%) ATC tumors (Figure 20A, B). No additional cases of *EML4-ALK* were found. Unlike *TP53* mutations, which are found exclusively in dedifferentiated tumors, *ALK* fusions are found in PTC as well as ATC and PDTC. The presence of *ALK* fusions in well-differentiated tumors indicates that *ALK* fusions are early events in tumor formation. Furthermore, significantly more *ALK* fusions were found in tumors with dedifferentiation ($P<0.05$, Fisher's exact test) (Figure 21A).

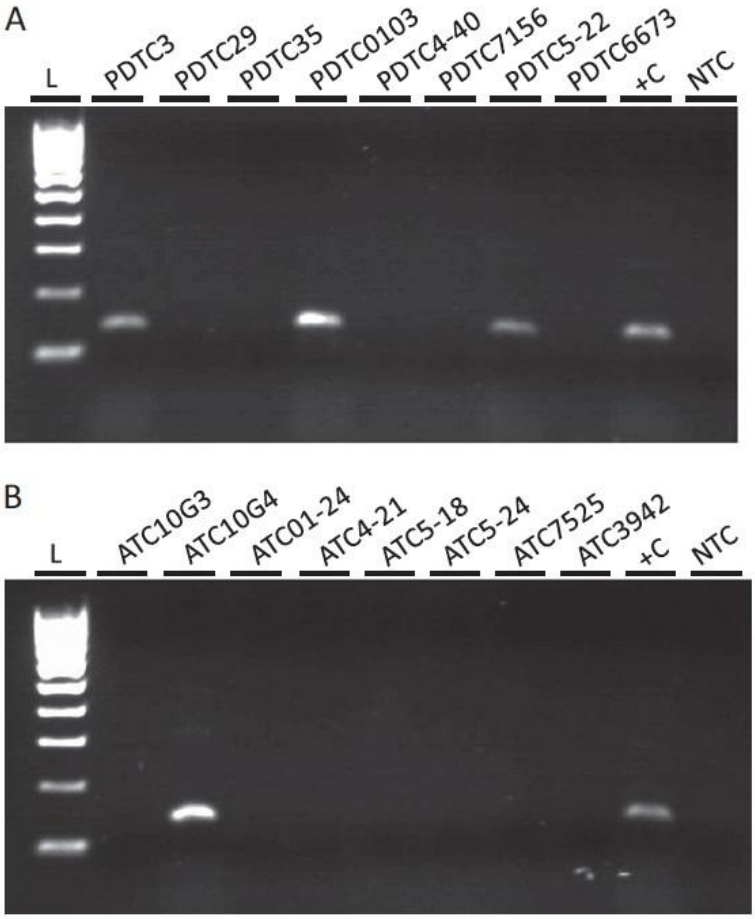

Figure 20: Detection of STRN-ALK transcripts in poorly differentiated thyroid carcinoma (PDTC) and anaplastic thyroid carcinoma (ATC).

Selected agarose gels from the RT-PCR screening of PDTC and ATC for STRN-ALK fusion. (A) STRN-ALK fusion was detected in three PDTCs. (B) STRN-ALK fusion was detected in one ATC. +C, positive control; L, 100-bp ladder; NTC, negative control.

Since *ALK* fusions were found more frequently in aggressive PDTC and ATC cases, *ALK* positive PTC cases were reviewed for any aggressive phenotypes. The H&E stained slides for ALK positive PTC cases showed tumors with a follicular growth pattern as expected in well-differentiated tumors. PTC cases positive for ALK fusions fell into two groups by histological

examination. Two of the four cases were TNM (tumor, node, metastasis) stage I-II with a predominate follicular growth pattern and focal papillary structures (Figure 21B). The second group held tumors with aggressive features including extrathyrodial extension and/or lymph node metastasis and presented at TNM stage III.

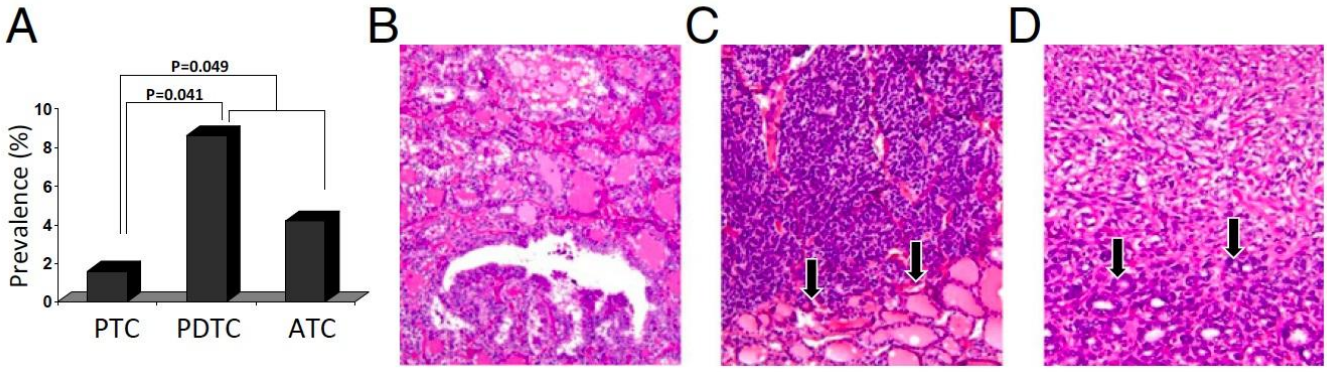

Figure 21: Prevalence and phenotypic features of thyroid cancer associated with ALK fusions.

(A) Prevalence of ALK fusions in PTC, PDTC, and ATC. (B) Well-differentiated PTC with a predominantly follicular growth pattern and focal papillary structures. (C) PDTC with areas of residual well-differentiated PTC with a follicular growth pattern (arrows). (D) ATC with a neighboring area of well-differentiated PTC with a follicular growth pattern (arrows). H&E stain. (Magnification: 100×).

Two of three PDTC tumors that were positive for STRN-ALK had areas of follicular growth pattern, indicating residual well-differentiated PTC (Figure 21C). These patients presented with wide spread disease. Similar to the PDTC tumors, the STRN-ALK fusion positive ATC tumor had residual areas of well-differentiated PTC (Figure 21D). Six months after diagnosis, this patient died of widely metastatic disease.

The eight tumors positive for *ALK* fusions, including PTC and dedifferentiated tumors, were negative for other known driver mutations. This includes *BRAF*, *RAS*, and fusions such as *RET/PTC*. None of these patients reported a history of radiation exposure. The lack of other driver events supports *ALK* fusions as the oncogene in these tumors. The phenotypic

characteristics of the *ALK* positive tumors indicate that *ALK* fusions occur in PTC tumors having follicular growth patterns. Furthermore, *ALK* fusions are found in dedifferentiated tumors that are likely to have formed directly from dedifferentiation of PTC tumors with follicular structures. The finding that *ALK* fusions are mutually exclusive with other known driver mutations in thyroid cancer and the presence of follicular variant of PTC structures in the tumors suggests that *ALK* fusions are independent driver events that may cause dedifferentiation of FV-PTC tumors.

Not only is *ALK* an important event in the progression of thyroid cancer, but it also represents a possible treatment target. As discussed above, PDTC and ATC patients have dismal outcomes due to the lack of response to traditional radioiodine treatment [28]. Only minimal progress has been attained using targeted treatments [50]. ALK inhibitors have gained FDA approval for treatment of ALK positive NSCLC and the second and third generations of ALK inhibitors designed with greater specificity are in clinical trials. These drugs represent a possible treatment option for patients with ALK positive aggressive thyroid cancers.

3.6 INHIBITION OF STRN-ALK INASE AND CELL GROWTH IN VITRO

3.6.1 Small molecule ALK inhibitors have been FDA approved for ALK positive NSCLC

Crizotinib (brand name Xalkori, produced by Pfiser) is an ATP-competitive inhibitor for ALK and MET [83]. Crizotinib was approved by the US Food and Drug Administration (FDA) for treatment of EML4-ALK positive NSCLC due to a significant response rate and low toxicity [84]. In the phase III trial comparing ALK positive NSCLC patients treated with crizotinib to those treated with chemotherapy, patients treated with crizotinib have an average progression-

free survival of 7.7 months and a response rate of 65% [85]. This is more than double the progression-free survival of 3.0 months in the chemotherapy group, which had a response rate of only 20% [85]. In addition, patients receiving crizotinib reported a significant quality of life improvement over treatment with chemotherapy in terms of both side effects from treatment and symptoms of lung cancer [85].

Second generation ALK inhibitors are being developed to overcome the most common mechanism of crizotinib resistance, an acquired mutation in ALK [86, 87]. Secondary mutations in *ALK* occur in ~22-33% of patients who develop resistance to crizotinib [88]. TAE684 was among the initial second generation ALK inhibitors tested to overcome resistance mutations and at the time of our *in vitro* inhibitor experiments was in clinical trials [89]. As potential drugs for the treatment of ALK positive thyroid cancer, we tested both crizotinib and TAE684 for their ability to inhibit the kinase activity of novel STRN-ALK fusions and block the cell proliferation advantage given by STRN-ALK in thyroid cells.

3.6.2 Crizotinib and TAE684 inhibit STRN-ALK kinase activity *in vitro*

We used a kinase assay to test the ability of ALK inhibitors to block the phosphorylation of a substrate *in vitro*. HA-tagged constructs for STRN-ALK, kinase dead STRN-ALK (K230M), and empty vector were transfected into HEK293 cells. Protein was isolated using IP for the HA-tag for each sample. We used a synthetic peptide YFF (Tyrosine-Phenylalanine-Phenylalanine) that was optimized and specific for ALK kinase [78]. STRN-ALK phosphorylates YFF in a kinase-dependent reaction, and linear pYFF product accumulation occurs for 20 min. (Figure 22A). Neither STRN-ALK (K230M) nor empty vector protein samples demonstrated the ability to phosphorylate the substrate confirming that the accumulation of pYFF is ALK kinase specific.

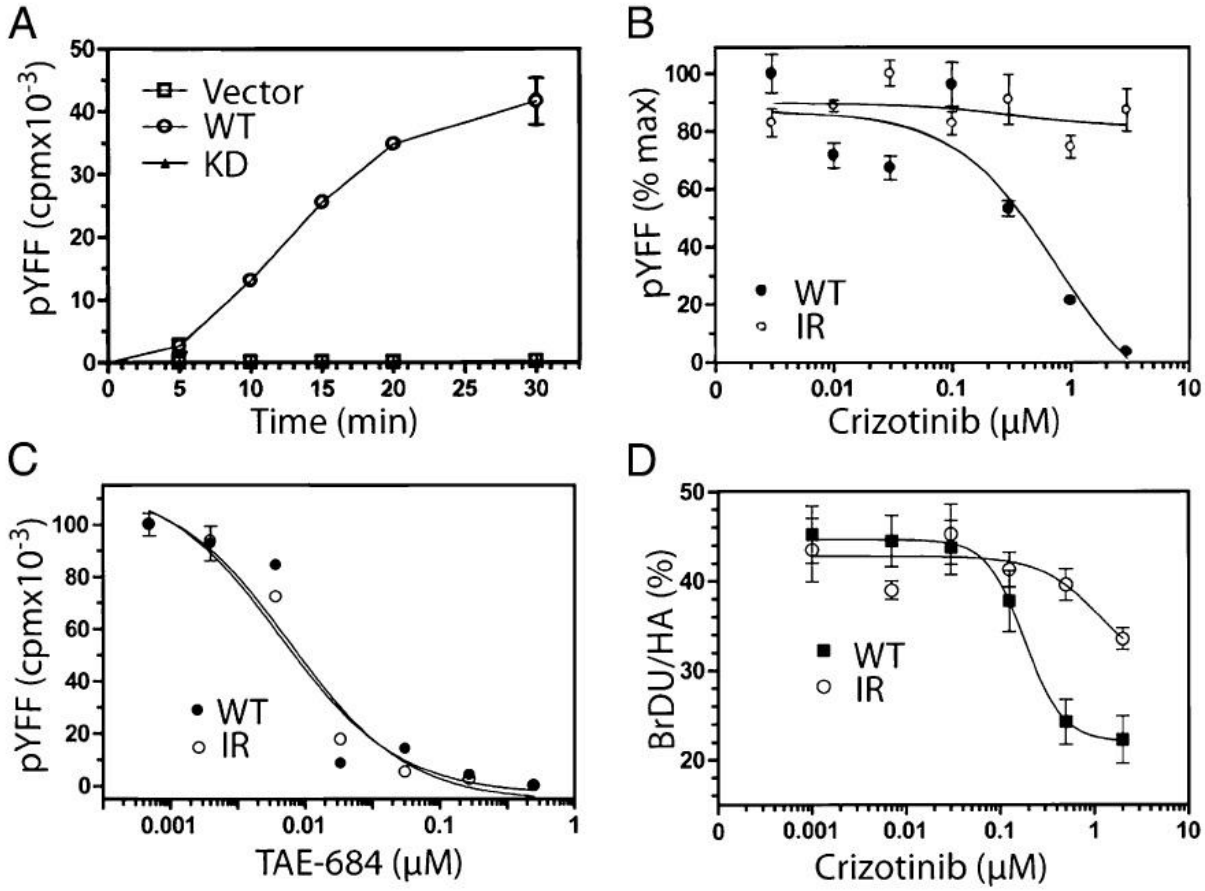

Figure 22: Inhibition of STRN-ALK kinase activity and thyroid cell growth by ALK inhibitors.

(A) Immunoprecipitation-coupled kinase assay from HEK-transfected cells using the synthetic YFF peptide substrate showing kinase-dependent YFF phosphorylation (pYFF) with linear product accumulation up to 20 min. KD, kinase-dead STRN-ALK (K230M); WT, STRN-ALK. Inhibition of substrate phosphorylation by crizotinib (B) and TAE684 (C) in HEK 293 cells expressing STRN-ALK (WT) and STRN-ALK (G349S) mutant (IR) measured at 15 min. (D) Inhibition of growth in PCCL3 thyroid cells expressing HA-STRN-ALK (WT) and HA-STRN-ALK (G349S) mutant (IR) by crizotinib. Cells cultured in cell media containing 5% (vol/vol) FBS and no TSH were treated with different concentrations of crizotinib for 24 h, and BrdU was added for the last 4 h of crizotinib treatment. Cell proliferation was assessed as a percentage of HA/BrdU-positive cells. Lines are the curve fitting to a dose–response curve.

Most patients with ALK positive NSCLC that are treated with crizotinib acquire resistance to the drug and suffer from disease progression. One common mechanism of

resistance is acquiring point mutations in the ALK fusion protein that decrease the ability of crizotinib to bind and inhibit kinase activity. A frequent mutation, in which a glycine (Gly1269 of the WT ALK) in the ATP-binding pocket is replaced with Ser, results in a loss of sensitivity to crizotinib but not to a diaminopyrimidine ALK inhibitor, TAE684 [89]. Glycine 1269, which is in position 349 in the fusion protein, was mutated in STRN-ALK (G349S) to create a HA-tagged STRN-ALK inhibitor resistant protein. As before, HEK293 cells were transfected with STRN-ALK and inhibitor resistant STRN-ALK (G349S) and protein was isolated by IP for the HA-tag. The production of pYFF at 15 min for each protein was measured to determine dose-response to crizotinib or TAE684. Crizotinib inhibited STRN-ALK with an IC_{50} ~250nM and STRN-ALK (G349S) mutant protein was resistant up to 3μM (Figure 22B). STRN-ALK (G349S) was inhibited by TAE684, and both STRN-ALK and the inhibitor resistant mutant had a similar dose response curve with an IC_{50} of ~8nM (Figure 22C).

3.6.3 Crizotinib inhibits *in vitro* cell proliferation in STRN-ALK expressing thyroid cells

After determining the sensitivity to ALK inhibitors using the kinase assay, we tested crizotinib for the ability to reduce cell proliferation in STRN-ALK positive thyroid cells. As demonstrated in Figure 19B above, STRN-ALK kinase activity caused TSH-independent cell proliferation in PCCL3 rat thyroid epithelial cells. PCCL3 cells were transfected with HA-tagged STRN-ALK and inhibitor resistant STRN-ALK (G349S). A BrdU assay was used to calculate cell proliferation in PCCL3 cells that expressed STRN-ALK or the inhibitor resistant mutant. The cells were cultured with different concentrations of crizotinib in the absence of TSH for 24 hrs. Crizotinib inhibited growth of the cells expressing STRN-ALK with an IC_{50} of ~0.2μM (Figure 22D). The IC_{50} of crizotinib for cells in culture was similar to the level determined by the kinase

assay. PCCL3 cells expressing STRN-ALK (G349S) were resistant to crizotinib concentrations below 2μM. This demonstrates that inhibition of STRN-ALK in thyroid cells blocks cell proliferation and raises the possibility for STRN-ALK to be a therapeutic target in thyroid cancer.

3.7 *IN VIVO* TESTING OF ALK INHIBITORS CRIZOTINIB AND LDK378

3.7.1 LDK378 is FDA approved for patients that have progressed on crizotinib

Although TAE684 was able to block ALK kinase activity effectively in *in vitro* and *in vivo* models, its use was discontinued in clinical trials in favor of newer ALK inhibitors due to liver toxicity [90]. There are several other inhibitors in clinical trials for ALK inhibition, including LDK378, also known as ceritinib and Zykadia (Novartis). LDK378 has recently received FDA approval for the treatment of patients with ALK-positive metastatic NSCLC who have progressed on crizotinib [91]. Like TAE684, LDK378 overcomes common resistance mutations in ALK to confer kinase inhibition, whereas crizotinib fails [92]. In order to identify the most efficacious treatment for STRN-ALK positive tumors we tested the ability of crizotinib and LDK378 to suppress STRN-ALK positive tumor growth using *in vivo* xenograft models.

3.7.2 Crizotinib and LDK378 stop the growth of STRN-ALK positive xenografts

Two ALK inhibitors have been FDA approved for treatment of tumors with ALK fusions in NSCLC. Crizotinib is the first inhibitor used, and if patients do not respond or have disease

progression with this treatment LDK378 is then used. Results of our *in vitro* testing indicate that both crizotinib and TAE684 are able to inhibit ALK kinase activity, blocking substrate phosphorylation. As TAE684 has been replaced in clinical trials, we selected LDK378 and crizotinib to test for their ability to halt tumor growth in xenograft models of *STRN-ALK* positive tumors.

To generate the xenograft tumors, we injected 1 x 10^5 NIH 3T3 mouse fibroblast cells expressing STRN-ALK subcutaneously into nude mice flanks. Tumors were measured daily with digital calipers. To more closely mimic treatment of human tumors, which are established in the patient at time of first treatment, xenografts were allowed to grow until they reached an average tumor volume of 400mm^3. When the tumors reached the appropriate size, mice were randomized into three treatment groups of crizotinib, LDK378, and vehicle; n=5 for each group. We treated the mice every 24 hours for seven consecutive days with 50mg/kg by oral gavage. Both crizotinib and LDK378 were able to stop the growth of the xenograft tumors (Figure 23A).

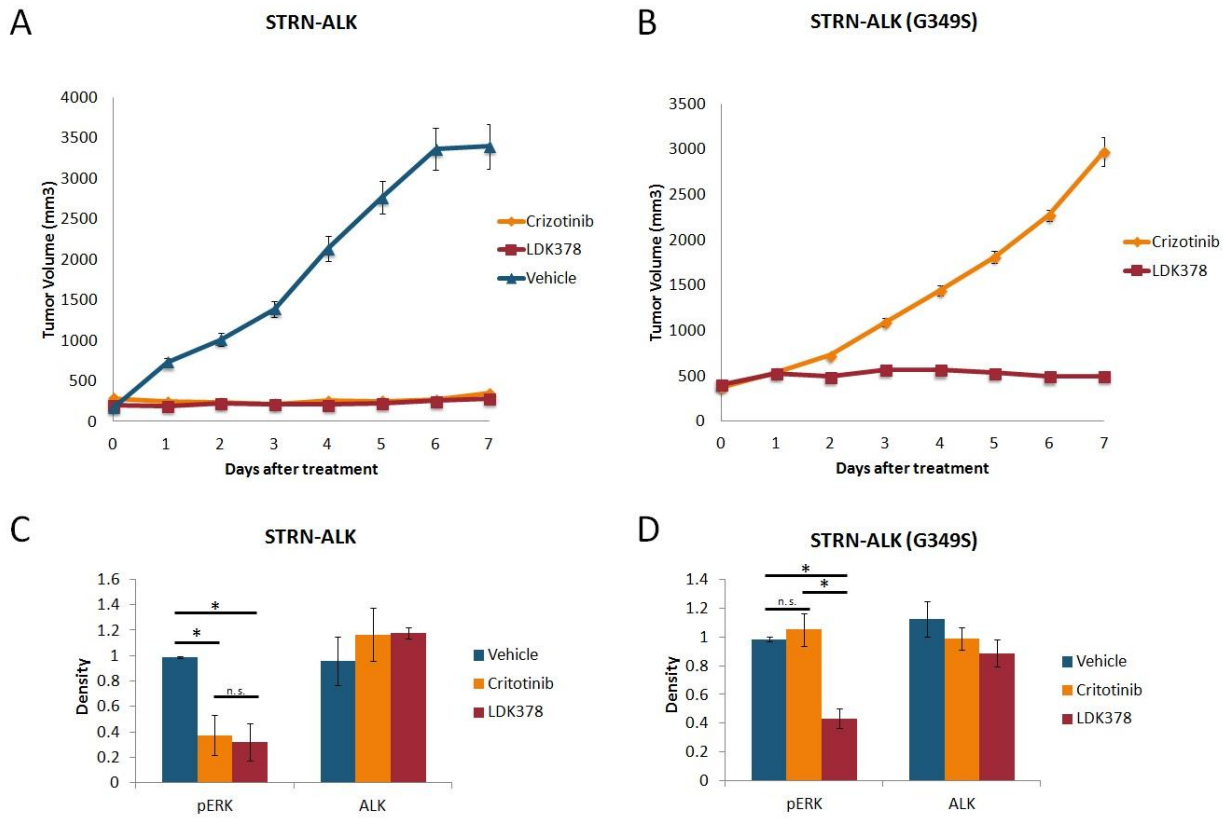

Figure 23: *In vivo* treatment of STRN-ALK and STRN-ALK (G349S) xenografts with ALK inhibitors

(A) Kinetics of tumor growth in xenografts of NIH 3T3 cells in nude mice injected s.c. in the flank with 1×10^5 cells expressing STRN-ALK and treated with crizotinib, LDK378, and vehicle; n=5 for each group. Mice were treated every 24 hours for 7 consecutive days with 50mg/kg by oral gavage. (B) Kinetics of tumor growth in xenografts of NIH 3T3 cells in nude mice injected s.c. in the flank with 1×10^5 cells expressing STRN-ALK (G349S), the inhibitor resistant mutation, and treated with crizotinib and LDK378; n=5 for each group. Mice were treated every 24 hours for 7 consecutive days with 50mg/kg by oral gavage. (C) Quantification of pERK compared to tERK and normalized to actin expression in STRN-ALK xenograft tumors 8 hours after 1 dose of crizotinib, LDK378, or vehicle; n=3, bars ± SE. (Student's t-test, $p<0.05$) (D) Quantification of pERK compared to tERK and normalized to actin expression in STRN-ALK (G349S), inhibitor resistant xenograft tumors 8 hours after 1 dose of crizotinib or LDK378; n=3, bars ± SE. (Student's t-test, $p<0.05$)

3.7.3 LDK378, but not crizotinib, inhibits tumor growth in tumors with an acquired resistance mutation

In addition to testing each inhibitor on tumors expressing STRN-ALK fusions, both inhibitors were used to treat STRN-ALK tumors that carry the G349S mutation. This mutation in the ATP binding pocket is thought to interfere with the ability of crizotinib to fill the pocket by steric hindrance [92]. As discussed above, G349S is a common mutation acquired in patient tumors, resulting in the loss of response to crizotinib. LDK378 has received FDA approval to treat patients that are unresponsive to crizotinib or progress while receiving crizotinib treatment. Since receiving approval, LDK378 has been demonstrated to be effective in inhibiting ALK fusions that harbor the G349S mutation.

To test LDK378 and crizotinib, we injected 1 x 10^5 NIH 3T3 mouse fibroblast cells expressing STRN-ALK (G349S) subcutaneously into the flanks of nude mice to generate the xenograft tumors as above. When the tumors reached 400mm^3 the mice were randomly assigned to treatment groups and treated every 24 hours with 50mg/kg of drug or vehicle for seven days. As anticipated, STRN-ALK (G349S) tumors continued to grow when treated with crizotinib but stopped growing upon treatment with LDK378 (Figure 23B). This was consistent with the MAPK pathway signaling results, as determined by western blot for pERK. In STRN-ALK tumors, pERK was significantly reduced by treatment with both crizotinib ($p=0.0178$) and LDK378 ($p=0.0107$), and there was no significant difference between the treatments ($p=0.8155$) (Figure 23C). Xenograft tumors positive for STRN-ALK (G349S) resistant to crizotinib had normal levels of pERK signaling but significantly reduced signaling when treated with LDK378 compared to vehicle ($p=0.0011$) and crizotinib ($p=0.0091$) (Figure 23D).

3.8 SUMMARY OF *IN VIVO* ALK INHIBITION

ATC and PDTC are among the most aggressive tumors to affect humans. These tumors have dedifferentiated and no longer take up iodine. Tumors that no longer respond to radioiodine have a 10% survival rate at ten years compared to 90% in patients whose tumors are radioiodine responsive [93]. STRN-ALK is an attractive target for ALK inhibitors for ATC and PDCA tumors. Patients with ALK positive NSCLC treated with crizotinib have increased progression free survival and a better quality of life as reported by the patients [85]. We have demonstrated that crizotinib is able to block the kinase activity of the novel STRN-ALK fusion. In an *in vitro* kinase activity assay, phosphorylation of the ALK substrate synthetic peptide is blocked by crizotinib and TAE684. Crizotinib reverses the increased TSH-independent cell proliferation in STRN-ALK positive PCCL3 rat epithelial cells, which are an *in vitro* model of normal thyroid cells that still require TSH for survival [81].

Patients treated with TKI inhibitors frequently develop resistance over time and new ALK inhibitors are currently in clinical trials [88]. We demonstrated that TAE684 blocks the kinase activity of STRN-ALK fusions and STRN-ALK (G349S), a mutation in the ATP binding pocket that results in inhibitor resistance [89, 92]. Aggressive dedifferentiated thyroid tumors have few treatment options, and the response of STRN-ALK positive thyroid cells *in vitro* suggests that crizotinib and second-generation ALK inhibitors could be used to treat ALK positive ATC and PDTC tumors.

To address the ability of orally available ALK small molecule inhibitors to block ALK *in vivo*, we generated STRN-ALK and STRN-ALK (G349S) xenograft tumors in nude mice. Crizotinib and LDK378 were used to treat mice by oral gavage for 7 days after the tumors have been established. LDK378, which replaced TAE684 in clinical trials, has recently received FDA

approval for patients that progress on crizotinib. Patients treated with LDK378 after being treated with crizotinib had a response rate of 56% [91]. Both crizotinib and LDK378 arrested the growth of STRN-ALK tumors of the *in vivo* xenograft model. As expected, xenograft tumors with STRN-ALK (G349S), a common resistance mutation found in ALK fusions after patients relapsed during crizotinib treatment, did not respond to crizotinib. LDK378 was able to overcome the resistance of STRN-ALK (G349S) and inhibited the growth of the xenograft tumors. Our preclinical *in vivo* data of xenograft tumors demonstrates that ALK inhibitors could be used to successfully treat patients with ALK positive thyroid cancer.

3.9 GENERATION OF TRANSGENIC MICE WITH THYROID-SPECIFIC STRN-ALK EXPRESSION

Transgenic mice provide a powerful tool to model tumor development and treatment of oncogenes. Our aim is to study the oncogenic properties *in vivo* of STRN-ALK expression in mouse thyroid cells. This will allow us to explore the function of STRN-ALK in several capacities. Although the xenograft model of STRN-ALK demonstrated the ability to form tumors and respond to ALK inhibition, xenografts are known to lack the ability to recapitulate tumor architecture and genetic heterogeneity [94]. Generation of STRN-ALK tumors in transgenic mice that dedifferentiate would validate the findings of ALK fusions in PDTC and ATC and provide confirmation that STRN-ALK is a driver event of thyroid cancer. STRN-ALK driven PDTC and ATC tumors in mice would also allow us to study the phenotypic features of dedifferentiation. In addition to studies of tumor progression, the STRN-ALK transgenic mouse will provide a

preclinical model for drug testing to study the affect of ALK inhibitors on *in vivo* STRN-ALK thyroid tumors.

3.9.1 Generation of STRN-ALK transgenic mice

To study thyroid specific expression of STRN-ALK, we designed an expression vector using the bovine-thyroglobulin (BTg) promoter for bicistronic expression of HA-STRN-ALK and fLuc-dsRed fusion protein (Figure 24A). The BTg promoter has been demonstrated previously to drive thyroid specific expression in mice [95, 96]. The fLuc-dsRed fusion protein combines the firefly luciferase with red fluorescence protein to allow *in vivo* bioluminescence imaging of developing thyroid tumors and metastasis [97]. Transgenic mice were prepared from the FVB/N strain at the University of Pittsburgh Magee Womens Research Institute Transgenic and Molecular Research Core. We identified three pups to be positive for the STRN-ALK transgene and used them to establish three independent lines. We checked expression of the transgenic mice using western blot for ALK and IF for HA, ALK, and dsRed expression (Figure 24B-D). All three lines express STRN-ALK and, though they have different levels of expression, it is similar to the level of STRN-ALK expressed in human thyroid tumors (Figure 24B). At this time we have selected lines 1 and 3 based on the expression data to proceed with extended aging and goitrogen treatments.

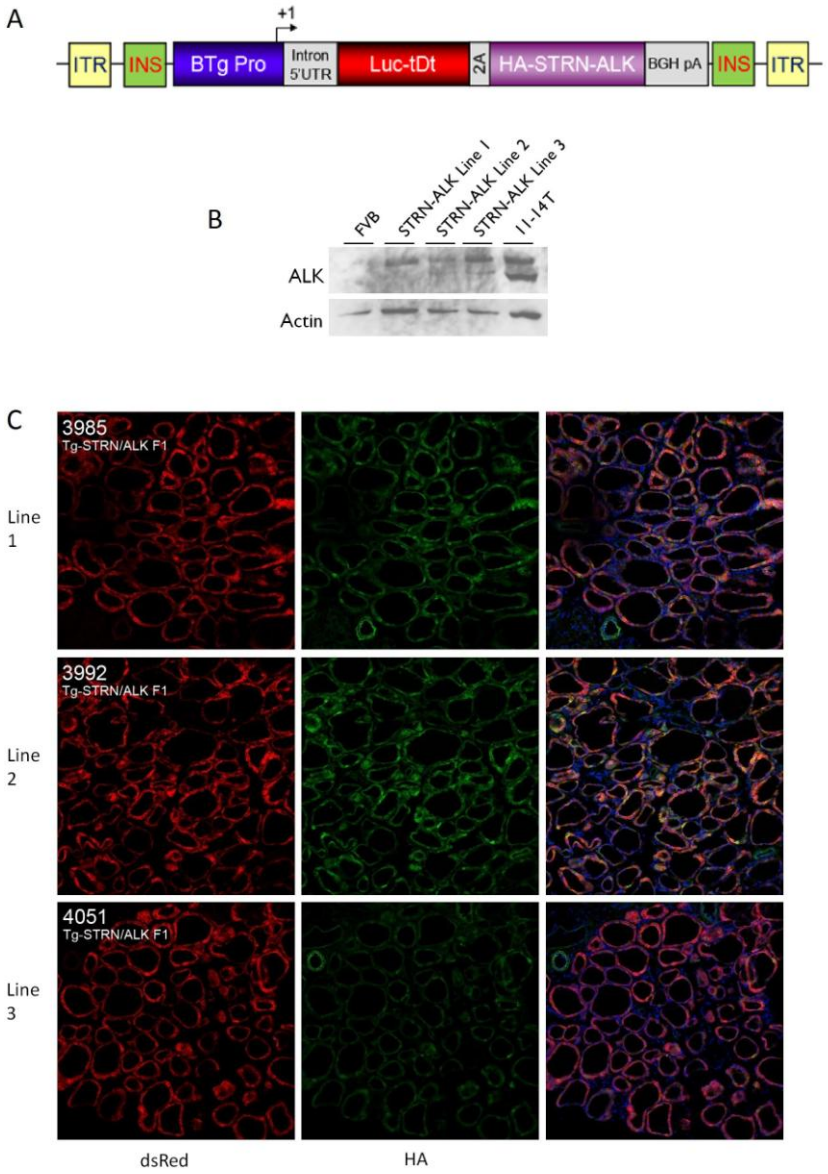

Figure 24: STRN-ALK transgenic mouse construct and expression

(A) Transgenic construct strategy. BTg Pro: bovine thyroglobulin promoter; 5'UTR: 5' non-coding region from HSV TK; HA-STRN-ALK: HA-tagged fusion protein; IRES: internal ribosome entry site; fLuc-dsRed: firefly luciferase-tandem tomato red fluorescent fusion; intron polyA: from rabbit β-globin. The unit is surrounded by a NotI sites that will be used to isolate the DNA fragment free of vector DNA for microinjection. (B) Western blot analysis of protein isolated from the transgenic mouse thyroid. STRN-ALK fusion protein is expressed at similar levels to the positive human tumor sample that is STRN-ALK positive. (C) Immunofluroscence of the dsRed (left), HA tag (Green, middle), and colocalization confirming the western blot results that all lines express STRN-ALK.

3.9.2 Current and future studies for STRN-ALK transgenic mice

The primary goal is to establish a phenotype and timeline of tumor development by aging the mice. As discussed above, the frequency of dedifferentiated tumors increases in populations with high incidence of goiter [33]. Recent epidemiological studies [98] and mouse studies [99] support the possible involvement of goiter or TSH stimulation in tumor initiation. Goiter can be mimicked in mice by subjecting the mice to a goitrogen-stimulation regime that raises TSH level > 50-fold. To determine the phenotype and any tumor development resulting from STRN-ALK expression in mouse thyroid, transgenic mice and STRN-ALK negative littermates will be aged with and without goitrogen treatment water for 3m, 6m, and 12m. An additional time point of 18m will be aged without goitrogen treatment. The thyroids will be collected from mice at each time point and then the tissue will be fixed and sectioned to determine tumor presence and phenotype.

Unlike well-differentiated tumors where mutations such as BRAF are mutually exclusive with other oncogenes, dedifferentiated tumors have accumulated many mutations, such as TP53. As more ALK positive human ATC and PDCA tumors are identified and characterized, it will be possible to select other transgenic mouse lines to breed with STRN-ALK mice to understand the roles of multiple mutations in tumor formation. This will also provide additional opportunities to correctly produce a phenocopy of ATC or PDTC.

Once the progression of the STRN-ALK tumors in transgenic mice has been clearly delineated, the goal will be to use this as a preclinical model to test inhibitor efficacy. The mice will be treated with FDA approved ALK inhibitors crizotinib and LKD378. In addition to the standard clinical therapies, we can begin to explore combined treatment with other therapeutic targets.

4.0 CONCLUSIONS AND FUTURE DIRECTIONS

From a pool of 446, 112 cases negative for known driver mutations in PTC were used to select a set of 21 cases for transcriptome sequencing. Using RNA-Seq we identified new fusions in thyroid cancer, *ALK* and *NTRK3*. *ALK* fusions result in aberrant expression of ALK tyrosine kinase that is activated in thyroid cells by ligand-independent autophosphorylation through STRN dimerization. These fusions impact important areas of thyroid cancer research and treatment.

ALK fusions increase our understanding of thyroid cancer pathogenesis. The higher prevalence of ALK fusions in dedifferentiated tumors suggests that this is an early event in tumorigenesis that may drive the dedifferentiation of PTC. ALK also presents a potential treatment target with readily available and FDA approved ALK inhibitors. Our preclinical data modeling the treatment of STRN-ALK fusions *in vitro* and *in vivo* confirms that STRN-ALK is a druggable target.

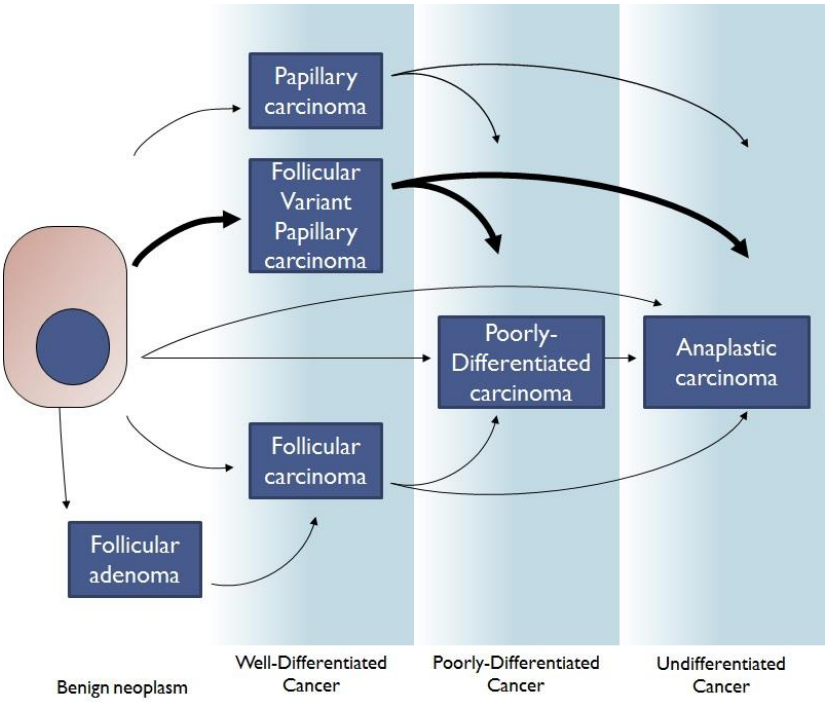

Figure 25: Step-wise dedifferentiation of follicular cells to thyroid cancer highlighting the follicular variant of papillary thyroid cancer.

Follicular cells of the thyroid undergo progression of dedifferentiation to become well-differentiated tumors and then poorly differentiated or anaplastic carcinoma. Our data indicate that *ALK* fusions occur in the follicular variant of papillary thyroid cancers that have aggressive phenotypes prone to dedifferentiation. PDTC and ATC tumors with ALK fusions show evidence of formation directly from dedifferentiation of PTC tumors with follicular structures. Adapted from (2)

In fact, there has been two published case reports of patients with aggressive ALK positive thyroid cancer treated with crizotinib. The first case was of an ATC that had a small component of FV-PTC; the tumor had invasion out of the capsule into the surrounding tissue and was metastatic [100]. Upon ALK positive IHC and FISH, the patient was treated with crizotinib and had a greater than 90% response at 3 and 6 months of treatment. The excellent response of this patient to crizotinib demonstrates that ALK inhibition is an effective treatment for ALK positive thyroid tumors. The second patient had aggressive PTC that did not respond to standard therapy and upon identification of an *EML4-ALK* fusion by whole-genome sequencing was

treated with crizotinib [101]. Although the patient had stable disease after 6 months of treatment, the authors felt that the patient did not respond and suggested that there may be a group of ATC patients with intrinsic resistance that will not respond to crizotinib [101].

One concept offering a new way to view progression and treatment is the cancer stem cell (CSC) hypothesis that suggests a smaller population cells within the tumor maintain the ability to replicate indefinitely (forum). The presence of CSCs in thyroid cancer is still debated [102]. In our model we propose that the dedifferentiation of STRN-ALK positive cells in FV-PTC tumors results in aggressive tumors that would respond to treatment with ALK inhibitors. However, if some or all of the CSC population are ALK negative treatment may only result in a temporary halt to tumor growth and the tumor will eventually be repopulated by the remaining CSCs. Another possibility is that cancer cells develop stem-like characteristics through dedifferentiation [103]. STRN-ALK expression or the resulting environment in ALK positive tumors may provide the conditions to generate CSCs from well-differentiated tumor cells. Regardless of the origin of the CSCs, successful treatment of the tumor may require treatment of cells with stem-like characteristics and their daughter cells. One recent study demonstrated that by targeting CSCs selectively while also using antitumor drugs to eliminate the majority of the tumor cells, glioblastomas were significantly inhibited from growth [104, 105].

In NSCLC, most patients treated with tyrosine kinase inhibitors (TKIs) develop acquired resistance within 1-2 years regardless of the inhibitor selected [88]. Acquired resistance can be grouped generally into two categories, pharmacological and biological resistance [86, 88, 106]. In acquired pharmacological resistance, the tumor may still respond to the drug, but inadequate drug exposure causes the patient to progress, such as a metastasis across the blood-brain barrier [88]. The most common form of biological resistance is a mutation in the RTK; ~22-33% of

tumors gain a resistance mutations such as G1269S (G349S in STRN-ALK) in ALK positive NCSLS. Although EGFR acquires resistance through a single gate-keeper mutation, at least 6 different ALK mutations have been identified in patients with resistance [88, 106]. Other mechanisms of resistance in ALK positive NSCLC include ALK amplification (6-16% of cases), increased EGFR signaling (30-35%), change in driver mutations (~5%), or KIT amplification (~10%) [86, 107, 108]. There is also a group of ALK positive NSCLC patients who seem to have intrinsic resistance and do not respond to crizotinib, the response rate is only ~65% [85].

LDK378, an FDA approved ALK inhibitor, has demonstrated a 56% response rate in patients who have progressed on crizotinib, but only a minority of those patients have ALK mutations to account for crizotinib failure [109]. Similar to crizotinib, which inhibits both ALK and MET, LDK378 inhibits ALK and insulin-like growth factor 1 receptor (IGF1R). In a recent publication, Lovly et al present an ALK positive NSCLC patient who first partially responded to an IGF1R-specific monoclonal antibody before also partially responding to crizotinib [109]. They suggest that this patient and their resulting *in vitro* data demonstrate the dual inhibition of ALK and IGF-1R by LDK378 may be greater than treatment with crizotinib alone. Similarly, Toyokawa et al describe an ALK positive lung adenocarcinoma patient who received three regimes of chemotherapy before a partial response to a second generation ALK inhibitor alectinib, followed by a "dramatic response" to crizotinib [110]. The metastatic lesion in the liver, which responded to crizotinib, was found to have amplification of *MET* by FISH suggesting that the combined MET and ALK inhibition from crizotinib created the response when ALK inhibition alone failed [110].

In both of these studies, the conclusions involving dual inhibition are the result of patients trying and failing multiple drug treatment regimens. Further work exploring this

interaction between ALK, IGF-1R and MET in a thyroid specific context will enhance our understanding of ALK driven ATC and PDTC tumors and aid in selection of the appropriate treatment for each patient. Our model of STRN-ALK tumors in transgenic mice could be exploited to study multiple treatment regimens. Crossing STRN-ALK mice with strains carrying mutations such as TP53, or over expressing other genes such as MET, will allow us to tailor the animal model to molecular profiles found in STRN-ALK positive ATC tumors.

The STRN-ALK and EML4-ALK fusions we identified in thyroid cancer relate directly to several challenges in the field: diagnosis of malignant tumors, treatment of aggressive dedifferentiated tumors, and understanding the mechanisms behind thyroid cancer pathogenesis and its growing incidence. Although further studies of the clinical application of ALK as a diagnostic marker in thyroid cancer are needed, ALK fusions represent novel molecular markers that can be screened for targeted, multigene panels being developed at UPMC and other leading institutes [111, 112]. The high prevalence of ALK fusions in aggressive tumors and the association of these fusions with aggressive FV-PTC tumors provides evidence that ALK fusions may be driving the dedifferentiation of certain types of PTC tumors. This moves us closer to understanding the pathogenesis of thyroid cancer. ALK is also a treatment target for dedifferentiated tumors that no longer respond to radioiodine, and FDA approved ALK inhibitors have been used to inhibit STRN-ALK for *in vitro* and *in vivo* models and successfully treat patients [100, 101, 113]. Our identification of EML4-ALK and novel STRN-ALK gene fusions represents a significant discovery in the field of thyroid cancer.

5.0 MATERIALS AND METHODS

5.1 SELECTION AND TESTING OF HUMAN THYROID TISSUE SPECIMENS

5.1.1 Tissue Samples and Nucleic Acid Isolation

Snap-frozen samples from tumor and normal-appearing thyroid tissue were collected using the protocol approved by the University of Pittsburgh Institutional Review Board or were provided by the University of Pittsburgh Health Sciences Tissue Bank with the appropriate patient consent obtained. RNA was isolated using Trizol reagent (Invitrogen) according to manufacturer's instructions. DNA was isolation using Qiagen DNeasy kit. Sample concentrations were determined using the NanoDrop (ThermoScientific).

5.1.2 RT-PCR, quantitative RT- PCR, and Sanger sequencing

Mutational analysis for BRAF codons 600 and 601, KRAS codons 12 and 13, HRAS codon 61, and NRAS codon 61 using real-time LightCycler PCR followed by fluorescence melting curve analysis and *RET/PTC1*, *RET/PTC3*, and *PAX8-PPARγ* using TaqMan real-time RT-PCR assays were performed as previously described [113] Briefly, for point mutations, each gene a pair of oligonucleotide primers flanking the mutation site was designed together with two fluorescent probes with the sensor probe spanning the codon of interest (TIB Molbiol, Berlin, Germany).

Amplification was performed for 35 cycles. Post amplification fluorescence melting curve analysis was performed by gradual heating of samples at a rate of 0.1 C/sec from 45 C to 95 C. For each mutation hot spot, DNA from a tumor or cell line known to carry a specific mutation was used as a positive control and DNA from peripheral blood lymphocytes was used as a wild-type negative control. Those samples that revealed no mutations in these hotspots, were further analyzed for mutations in the entire exon 15 of the BRAF gene, exon 2 of NRAS and HRAS, and exon 1 of KRAS using Sanger sequencing. Specifically, PCR amplification was performed using 25 ng of DNA and AmpliTaq Gold PCR Master Mix (Applied Biosystems, Inc, Foster City, CA). The PCR products were sequenced using the BigDye Terminator v3.1 Cycle Sequencing kit (Applied Biosystems). For *RET/PTC1*, *RET/PTC3*, and *PAX8-PPARɣ,* reverse transcription and PCR amplification were performed in one-step using QuantiTech Probe RT-PCR Kit (Qiagen) and gene-specific primers and probes. The reverse transcription was carried out at 50 C for 30 min, followed by 40-cycle PCR amplification.

For detection of new fusions from RNA-Seq, primers were designed using Primer3 (http://biotools.umassmed.edu/bioapps/primer3_www.cgi). Reverse transcription was performed using 1ug of RNA and the High-Capacity cDNA Reverse Transcription Kit (Life Technologies). The PCR was performed using Qiagen HotStarTaq DNA Polymerase as per manufactures recommendations and analyzed using 2% agarose gel.

5.2 RNA-SEQ SAMPLE PREPARATION, DATA ANLYSIS, AND VALIDATION

5.2.1 RNA-Seq library preparation and quantification

Tumor RNA samples were processed to remove ribosomal RNA using a Ribozero Magnetic Gold Kit (Illumina), followed by library preparation for RNA sequencing using an Illumina TruSeq RNA Sample Preparation Kit, version 2. The prepared libraries were assessed using an Agilent Bioanalyzer and a High Sensitivity DNA Kit (Agilent). Paired-end sequencing was performed on an Illumina HiSeq2000 sequencing system at the High-Throughput Genome Center at the Department of Pathology, University of Pittsburgh.

5.2.2 Data analysis of RNA-Seq results

Before the analysis, the adapter sequences were removed from the output reads by the tool cutadapt (http://code.google.com/p/cutadapt/); sequences with low quality (base quality <13) at both ends of reads were further trimmed, and trimmed reads with less than 25 bp were removed using SolexaQA (http://solexaqa.sourceforge.net/). A search for gene fusion events was performed using the ChimeraScan and deFuse \ programs. The trimmed sequence reads were aligned to the reference human genome (National Center for Biotechnology Information build 37.1) and gene annotation database (Ensembl genes v69 and University of California Santa Cruz genes hg19) by Bowtie in ChimeraScan \ and Genomic Short-read Nucleotide Alignment Program (GSNAP) in deFuse. In each program, the tumor and its matched normal thyroid sample were analyzed separately. All fusion events in tumors that were detected in their matched normal samples were filtered out. Then, the predicted fusion events from the two programs were

integrated and combined with genomic annotation to generate a list of candidate gene fusions. To reduce false-positive findings, the fusion events detected by both programs were further narrowed down by excluding (i) fusion events between adjacent genes (called as read-through); (ii) fusion events with no supporting reads spanning the predicted breakpoints; (iii) fusion events predicted to have five or more fusion partners and lacking specificity of target regions; and (iv) none of fusion partners presented in any of the three databases, including cancer Gene Census (http://www.sanger.ac.uk/research/projects/cancergenome/census.html), Mitelman genes (cgap.nci.nih.gov/chromosomes/Mitelman), and kinase genes (kinase.com/).

5.2.3 FISH

FISH was performed as previously reported [113]. To confirm the presence of ALK rearrangements, FISH was performed on 4-μm paraffin sections using the Vysis LSI ALK Dual Color Break Apart rearrangement probe (Abbott Molecular). To confirm the presence of ALK and striatin (STRN) gene fusion, FISH was performed on tumor touch preparations using the probes generated from BAC clones RP11-288C18 and RP11-547I5 labeled with SpectrumGreen-dUTP (Abbott Molecular) for STRN and from BAC clone RP11-328L16 labeled with SpectrumOrange-dUTP (Abbott Molecular) for ALK. All BAC clones were purchased from BACPAC Resources Center (Children's Hospital, Oakland, CA). Microscopy was performed using a Leica SP5 TCS 4D confocal laser scanning fluorescence microscope with digital image capture.

5.2.4 Immunohistochemistry

Immunohistochemistry was performed on 4-μm formalin-fixed and paraffin-embedded tissues sections using a BenchMark Ultra instrument, version 4 (Ventana). The primary rabbit monoclonal anti-ALK antibody (clone D5F3; Cell Signaling Technology) was used at a 1:100 dilution.

5.3 CELL CULTURE AND ASSAYS

5.3.1 Expression Vectors and Cell Transfection.

As previously reported [113], the full length ORF of the STRN-ALK fusion and inhibitor resistant mutant constructs were synthesized by GenScript (Clontech), cloned in pLVX-IRES-Puro plasmid, and Sanger sequenced to confirm accuracy. NIH 3T3 cells were transfected my adding 3uL X-tremeGENE HP Reagent (Roche Applied Science) and 1μg of each plasmid DNA in 100μL of Opti-MEM reduced serum media (Life Technologies) to each well of a 6-well cell culture plate.

5.3.2 Cell Culture and ALK inhibitors

Cells were maintained at 37 °C in a 5% CO2/95% humidified air environment. NIH 3T3 STRN-ALK cells were grown in DMEM supplemented with 10% FBS, 1% L-glutamine, and 1%

penicillin/streptomycin (Life Technologies). Crizotinib (PF-02341066) and LDK-378 (ceritinib) were purchased from Selleckchem and dissolved in DMSO (Sigma).

5.3.3 Western Blotting

Protein was isolated from snap-frozen tumor tissue homogenized in chilled radioimmunoprecipitation assay (RIPA) buffer (Boston BioProducts) with protease inhibitors (Roche) and phosphatase inhibitors (Sigma) using the OMNI-GLH homogenizer with hard tissue tips (OMNI International), incubated on ice for 30 min, and centrifuged at 15,000x*g* for 20 min at 4 °C; the supernatant was then collected. Protein concentration was determined using a BCA Protein Assay Kit (Pierce). Samples were resolved by SDS/PAGE (BioRad), transferred to a nitrocellulose membrane (BioRad), and immunoblotted with antibodies from Cell Signaling [ALK (D5F3) XP Rabbit (catalog no. 3633), phospho-ALK (Tyr1278; catalog no. 3710), p42/44 MAPK (catalog no. 9102), and phospho-p42/44 MAPK (pT202/pY204; catalog no. 9101)] and with **β**-actin (catalog no. A5441) from Sigma.

5.3.4 Cell Growth, Transformation, and Tumorigenicity Assays

The rate of cell proliferation was assessed in PCCL3 cells using BrdU labeling. For this, cells were grown to 60% confluency on glass coverslips, transfected with HA-STRN-ALK and control vectors for 24 h, and made quiescent by TSH starvation in Coon's modified F-12 medium/5% FBS for 16 h, followed by BrdU labeling (100 μM; Sigma) for 2 h. At the end of the labeling period, cells were fixed in 4% paraformaldehyde [10 min at room temperature (RT)] and permeabilized with 0.5% Triton X-100 (20 min at RT). After washing, incorporated BrdU was

detected by indirect immunofluorescence. Samples were costained for 1 h at RT with sheep anti-BrdU antibody (1:100 ratio; Biodesign International) and HA antibody (HA-11, 1:400 ratio, Covance) in PBS, 1% BSA, 5 mM MgCl2, and 1 mM CaCl2 containing RQ1 DNase (10 units/mL; Promega). After washes in PBS, 1% BSA, and 0.1% Tween 20, samples were incubated for 1 h at RT with a combination of Alexa 488-conjugated goat anti-sheep and Alexa 594-conjugated anti-mouse antibodies, containing 0.2 μg/mL DAPI (Sigma). After extensive washes in PBS and 0.1% Tween 20, samples were mounted in PermaFluor (Thermo) and viewed by epifluorescence (magnification of 60×). For the in vivo tumorigenicity assay, transiently transfected NIH 3T3 cells and nontransfected cells were injected s.c. into nude mice with equal parts Cultrex® Basement Membrane Extract, Type 3 (Trevigen). Tumor formation was monitored, and size was measured with a digital caliper. To establish cell lines, tumors were removed, washed with PBS containing 1% penicillin/streptomycin and digested with trypsin, collagenase, and hyaluronidase at concentrations recommended by manufacturer (Life Technologies). Isolated cells were plated and cultured as normal. ALK expression in established cells lines were confirmed by immunoblotting for HA and ALK.

5.3.5 Dimerization Assay

HEK 293 cells were cotransfected as described above with Myc-STRN-ALK and HA-STRN-ALK mutants, as indicated. At 24 h, cells were washed once with 1× PBS, and lysed in 500 μL per well of lysis buffer [50 mM Tris·HCl (pH 7.5), 150 mM NaCl, 10% glycerol, 0.5% Nonidet P-40 (Roche), 1 mM β-glycerophosphate, 1mMPMSF, 50mMNaF, 2mMorthovanadate, and protease inhibitor mixture set I (Calbiochem)]. Lysates were passed through a 27-gauge needle, left on ice for 10 min, and centrifuged for 15 min at 4 °C. An aliquot (20 μL) of supernatant was

kept as total lysate, and 0.5 μL of Myc antibody (9E10) was added to the tube for immunoprecipitation. After 1 h at 4 °C, 40 μL of A/G agarose beads was added and incubated for another hour on ice. Beads were washed three times in 1 mL of lysate buffer, and samples were run on SDS/PAGE and blotted for Myc and HA. Immunoprecipitation Coupled-Kinase Assay. HEK 293 cells were transfected with HA-STRN-ALK (WT and K230M) as described above. Samples were immunoprecipitated with HA antibody (HA.11) in lysis buffer, and beads were washed three times in 1 mL of lysis buffer, followed by two times in 1 mL of kinase buffer [50 mM Tris (pH 7.5), 5 mM MnCl2, 10 mMβ-glycerophosphate, 1 mM PMSF, and 1 mM DTT]. After the last wash, 50 μL of prewarmed (30 °C) kinase buffer containing 300 μM YFF (Tyrosine–Phenylalanine–Phenylalanine) peptide substrate (Ohio Peptide) and ATP mix (50 μM–4,000 cpm/pmol) was added to the beads and incubation was continued for the specified time at 30 °C. Aliquots (in duplicates) were spotted on P81 phosphocellulose squares, followed by five washes with 400 mL of 75 mM O-phosphoric acid and a final acetone wash before drying and counting. For ALK inhibitors' dose–responses, drugs were added for 20 min in kinase buffer before addition of YFF/ATP mix and further incubation for 15 min at 30 °C.

BIBILIOGRAPHY

1. Society, A.C., *Cancer Facts & Figures 2011*. 2011: Atlanta GA.
2. Nikiforov, Y.E. and M.N. Nikiforova, *Molecular genetics and diagnosis of thyroid cancer.* Nat Rev Endocrinol, 2011. **7**(10): p. 569-80.
3. Davies, L. and H.G. Welch, *Current thyroid cancer trends in the United States.* JAMA Otolaryngol Head Neck Surg, 2014. **140**(4): p. 317-22.
4. Zhu, Z., et al., *Molecular Profile and Clinical-Pathologic Features of the Follicular Variant of Papillary Thyroid Carcinoma: An Unusually High Prevalence of ras Mutations.* American Journal of Clinical Pathology, 2003. **120**(1): p. 71-77.
5. Albores-Saavedra, J., et al., *Changing patterns in the incidence and survival of thyroid cancer with follicular phenotype--papillary, follicular, and anaplastic: a morphological and epidemiological study.* Endocr Pathol, 2007. **18**(1): p. 1-7.
6. Colonna, M., et al., *A time trend analysis of papillary and follicular cancers as a function of tumour size: a study of data from six cancer registries in France (1983-2000).* Eur J Cancer, 2007. **43**(5): p. 891-900.

7. McFadden, D.G., et al., *Identification of oncogenic mutations and gene fusions in the follicular variant of papillary thyroid carcinoma.* J Clin Endocrinol Metab, 2014. **99**(11): p. E2457-62.

8. Ahn, H.S., H.J. Kim, and H.G. Welch, *Korea's Thyroid-Cancer "Epidemic" — Screening and Overdiagnosis.* New England Journal of Medicine, 2014. **371**(19): p. 1765-1767.

9. Chen, A.Y., A. Jemal, and E.M. Ward, *Increasing incidence of differentiated thyroid cancer in the United States, 1988-2005.* Cancer, 2009. **115**(16): p. 3801-7.

10. Banach, R., *Davies and Welch draw unfounded conclusions about thyroid cancer from epidemiological data.* JAMA Otolaryngol Head Neck Surg, 2014. **140**(7): p. 678-9.

11. Cancer Genome Atlas Research, N., *Integrated genomic characterization of papillary thyroid carcinoma.* Cell, 2014. **159**(3): p. 676-90.

12. Soares, P., et al., *BRAF mutations and RET/PTC rearrangements are alternative events in the etiopathogenesis of PTC.* Oncogene, 2003. **22**(29): p. 4578-80.

13. Davies, H., et al., *Mutations of the BRAF gene in human cancer.* Nature, 2002. **417**(6892): p. 949-54.

14. Caudill, C.M., et al., *Dose-dependent generation of RET/PTC in human thyroid cells after in vitro exposure to gamma-radiation: a model of carcinogenic chromosomal rearrangement induced by ionizing radiation.* J Clin Endocrinol Metab, 2005. **90**(4): p. 2364-9.

15. Nikiforov, Y., D.R. Gnepp, and J.A. Fagin, *Thyroid lesions in children and adolescents after the Chernobyl disaster: implications for the study of radiation tumorigenesis.* J Clin Endocrinol Metab, 1996. **81**(1): p. 9-14.

16. Leeman-Neill, R.J., et al., *ETV6-NTRK3 is a common chromosomal rearrangement in radiation-associated thyroid cancer.* Cancer, 2014. **120**(6): p. 799-807.

17. Nikiforov, Y.E., et al., *Distinct Pattern of ret Oncogene Rearrangements in Morphological Variants of Radiation-induced and Sporadic Thyroid Papillary Carcinomas in Children.* Cancer Research, 1997. **57**: p. 1690-1694.

18. Leeman-Neill, R.J., et al., *RET/PTC and PAX8/PPARgamma chromosomal rearrangements in post-Chernobyl thyroid cancer and their association with iodine-131 radiation dose and other characteristics.* Cancer, 2013. **119**(10): p. 1792-9.

19. Ciampi, R., et al., *Oncogenic AKAP9-BRAF fusion is a novel mechanism of MAPK pathway activation in thyroid cancer.* Journal of Clinical Investigation, 2005. **115**(1): p. 94-101.

20. Kroll, T.G., et al., *PAX8-PPARgamma1 fusion oncogene in human thyroid carcinoma [corrected]*. Science, 2000. **289**(5483): p. 1357-60.

21. Giordano, T.J., et al., *Delineation, functional validation, and bioinformatic evaluation of gene expression in thyroid follicular carcinomas with the PAX8-PPARG translocation.* Clin Cancer Res, 2006. **12**(7 Pt 1): p. 1983-93.

22. Ikawa, S., et al., *B-raf, a new member of the raf family, is activated by DNA rearrangement.* Mol Cell Biol, 1988. **8**(6): p. 2651-4.

23. Lee, N.V., et al., *A Novel SND1-BRAF Fusion Confers Resistance to c-Met Inhibitor PF-04217903 in GTL16 Cells though MAPK Activation.* PLoS ONE, 2012. **7**(6): p. e39653.

24. Uzman, A., *Molecular Cell Biology (4th edition) - Harvey Lodish, Arnold Berk, S. Lawrence Zipursky, Paul Matsudaira, David Baltimore and James Darnell; Freeman*

& Co., New York, NY, 2000, 1084 pp., list price $102.25, ISBN 0-7167-3136-3. Biochemistry and Molecular Biology Education, 2001: p. 126-128.

25. Greco, A., C. Miranda, and M.A. Pierotti, *Rearrangements of NTRK1 gene in papillary thyroid carcinoma.* Mol Cell Endocrinol, 2010. **321**(1): p. 44-9.

26. Groussin, L. and J.A. Fagin, *Significance of BRAF mutations in papillary thyroid carcinoma: prognostic and therapeutic implications.* Nat Clin Pract End Met, 2006. **2**(4): p. 180-181.

27. Deshpande, H.A., S. Roman, and J.A. Sosa, *New targeted therapies and other advances in the management of anaplastic thyroid cancer.* Curr Opin Oncol, 2013. **25**(1): p. 44-9.

28. Nikiforov, Y.E., P.W. Biddinger, and L.D.R. Thompson, *Diagnostic Pathology and Molecular Genetics of the Thyroid*. Second ed. 2012, Philadelphia: Wolters Kluwer Health | Lippincott Williams & Wilkins.

29. Volante, M., et al., *Poorly differentiated thyroid carcinoma: the Turin proposal for the use of uniform diagnostic criteria and an algorithmic diagnostic approach.* Am J Surg Pathol, 2007. **31**(8): p. 1256-64.

30. Smallridge, R.C. and J.A. Copland, *Anaplastic Thyroid Carcinoma: Pathogenesis and Emerging Therapies.* Clinical Oncology, 2010. **22**(6): p. 486-497.

31. Pettersson, B., et al., *Iodine supplementation in Sweden and regional trends in thyroid cancer incidence by histopathologic type.* Int J Cancer, 1996. **65**(1): p. 13-9.

32. Bakiri, F., et al., *The relative roles of endemic goiter and socioeconomic development status in the prognosis of thyroid carcinoma.* Cancer, 1998. **82**(6): p. 1146-53.

33. Hundahl, S.A., et al., *Initial results from a prospective cohort study of 5583 cases of thyroid carcinoma treated in the united states during 1996. U.S. and German Thyroid*

Cancer Study Group. An American College of Surgeons Commission on Cancer Patient Care Evaluation study. Cancer, 2000. **89**(1): p. 202-17.

34. Albores-Saavedra, J., et al., *Histologic variants of papillary and follicular carcinomas associated with anaplastic spindle and giant cell carcinomas of the thyroid: an analysis of rhabdoid and thyroglobulin inclusions.* Am J Surg Pathol, 2007. **31**(5): p. 729-36.
35. Aldinger, K.A., et al., *Anaplastic carcinoma of the thyroid: a review of 84 cases of spindle and giant cell carcinoma of the thyroid.* Cancer, 1978. **41**(6): p. 2267-75.
36. Papotti, M., et al., *Poorly differentiated thyroid carcinomas with primordial cell component. A group of aggressive lesions sharing insular, trabecular, and solid patterns.* Am J Surg Pathol, 1993. **17**(3): p. 291-301.
37. Pietribiasi, F., et al., *Cytologic features of poorly differentiated 'insular' carcinoma of the thyroid, as revealed by fine-needle aspiration biopsy.* Am J Clin Pathol, 1990. **94**(6): p. 687-92.
38. Bacher-Stier, C., et al., *Incidence and clinical characteristics of thyroid carcinoma after iodine prophylaxis in an endemic goiter country.* Thyroid, 1997. **7**(5): p. 733-41.
39. Kebebew, E., et al., *Anaplastic thyroid carcinoma.* Cancer, 2005. **103**(7): p. 1330-1335.
40. Volante, M., et al., *RAS Mutations Are the Predominant Molecular Alteration in Poorly Differentiated Thyroid Carcinomas and Bear Prognostic Impact.* The Journal of Clinical Endocrinology & Metabolism, 2009. **94**(12): p. 4735-4741.
41. Kitamura, Y., et al., *Immediate causes of death in thyroid carcinoma: clinicopathological analysis of 161 fatal cases.* J Clin Endocrinol Metab, 1999. **84**(11): p. 4043-9.
42. Hou, P., et al., *Genetic alterations and their relationship in the phosphatidylinositol 3-kinase/Akt pathway in thyroid cancer.* Clin Cancer Res, 2007. **13**(4): p. 1161-70.

43. Xing, M., *BRAF mutation in papillary thyroid cancer: pathogenic role, molecular bases, and clinical implications.* Endocr Rev, 2007. **28**(7): p. 742-62.

44. Catalano, M.G., et al., *Emerging molecular therapies of advanced thyroid cancer.* Mol Aspects Med, 2010. **31**(2): p. 215-26.

45. Fagin, J.A., et al., *High prevalence of mutations of the p53 gene in poorly differentiated human thyroid carcinomas.* J Clin Invest, 1993. **91**(1): p. 179-84.

46. Dobashi, Y., et al., *Stepwise participation of p53 gene mutation during dedifferentiation of human thyroid carcinomas.* Diagn Mol Pathol, 1994. **3**(1): p. 9-14.

47. Byrd, J.K., et al., *Well differentiated thyroid carcinoma: current treatment.* Curr Treat Options Oncol, 2012. **13**(1): p. 47-57.

48. Pinto, N., et al., *Genomically driven precision medicine to improve outcomes in anaplastic thyroid cancer.* J Oncol, 2014. **2014**: p. 936285.

49. Hogan, T., et al., *Oncocytic, focally anaplastic, thyroid cancer responding to erlotinib.* J Oncol Pharm Pract, 2009. **15**(2): p. 111-7.

50. Wu, H., et al., *Anaplastic Thyroid Cancer: Outcome and the Mutation/Expression Profiles of Potential Targets.* Pathol Oncol Res, 2015.

51. Savvides, P., et al., *Phase II trial of sorafenib in patients with advanced anaplastic carcinoma of the thyroid.* Thyroid, 2013. **23**(5): p. 600-4.

52. Wittwer, C.T., et al., *Continuous fluorescence monitoring of rapid cycle DNA amplification. 1997.* Biotechniques, 2013. **54**(6): p. 314-20.

53. Schroeder, A., et al., *The RIN: an RNA integrity number for assigning integrity values to RNA measurements.* BMC Molecular Biology, 2006. **7**(1): p. 3.

54. McPherson, A., et al., *deFuse: an algorithm for gene fusion discovery in tumor RNA-Seq data.* PLoS Comput Biol, 2011. **7**(5): p. e1001138.

55. Maher, C.A., et al., *Chimeric transcript discovery by paired-end transcriptome sequencing.* Proc Natl Acad Sci U S A, 2009. **106**(30): p. 12353-8.

56. Maher, C.A., et al., *Transcriptome sequencing to detect gene fusions in cancer.* Nature, 2009. **458**(7234): p. 97-101.

57. Knezevich, S.R., et al., *A novel ETV6-NTRK3 gene fusion in congenital fibrosarcoma.* Nature Genetics, 1998. **18**: p. 184-187.

58. Eguchi, M., et al., *Fusion of ETV6 to Neurotrophin-3 Receptor TRKC in Acute Myeloid Leukemia With t(12;15)(p13;q25).* Blood 1999. **93**(4): p. 1355-1363.

59. Rubin, B.P., et al., *Congenital Mesoblastic Nephroma t(12;15) Is Associated with ETV6-NTRK3 Gene Fusion: Cytogenetic and Molecular Relationship to Congenital (Infantile) Fibrosarcoma.* American Journal of Pathology, 1998. **153**(5): p. 1451-1458.

60. Tognon, C.E., et al., *The Chimeric Protein Tyrosine Kinase ETV6-NTRK3 Requires both Ras-Erk1/2 and PI3-Kinase-Akt Signaling for Fibroblast Transformation.* Cancer Research, 2001. **61**: p. 8909-8916.

61. Tognon, C.E., et al., *Mutations in the SAM domain of the ETV6-NTRK3 chimeric tyrosine kinase block polymerization and transformation activity.* Mol Cell Biol, 2004. **24**(11): p. 4636-50.

62. Morris, S.W., et al., *Fusion of a kinase gene, ALK, to a nucleolar protein gene, NPM, in non-Hodgkin's lymphoma.* Science, 1995. **267**(5196): p. 316-7.

63. Soda, M., et al., *Identification of the transforming EML4-ALK fusion gene in non-small-cell lung cancer.* Nature, 2007. **448**(7153): p. 561-6.

64. Roskoski, R., Jr., *Anaplastic lymphoma kinase (ALK): structure, oncogenic activation, and pharmacological inhibition.* Pharmacol Res, 2013. **68**(1): p. 68-94.

65. Moog-Lutz, C., et al., *Activation and inhibition of anaplastic lymphoma kinase receptor tyrosine kinase by monoclonal antibodies and absence of agonist activity of pleiotrophin.* J Biol Chem, 2005. **280**(28): p. 26039-48.

66. Castets, F., et al., *A novel calmodulin-binding protein, belonging to the WD-repeat family, is localized in dendrites of a subset of CNS neurons.* J Cell Biol, 1996. **134**(4): p. 1051-62.

67. Breitman, M., et al., *The armadillo repeat domain of the APC tumor suppressor protein interacts with Striatin family members.* Biochim Biophys Acta, 2008. **1783**(10): p. 1792-802.

68. Moqrich, A., et al., *Cloning of human striatin cDNA (STRN), gene mapping to 2p22-p21, and preferential expression in brain.* Genomics, 1998. **51**(1): p. 136-9.

69. Castets, F., et al., *Zinedin, SG2NA, and striatin are calmodulin-binding, WD repeat proteins principally expressed in the brain.* J Biol Chem, 2000. **275**(26): p. 19970-7.

70. Gaillard, S., et al., *Striatin, a calmodulin-dependent scaffolding protein, directly binds caveolin-1.* FEBS Lett, 2001. **508**(1): p. 49-52.

71. Goudreault, M., et al., *A PP2A phosphatase high density interaction network identifies a novel striatin-interacting phosphatase and kinase complex linked to the cerebral cavernous malformation 3 (CCM3) protein.* Mol Cell Proteomics, 2009. **8**(1): p. 157-71.

72. Gordon, J., et al., *Protein phosphatase 2a (PP2A) binds within the oligomerization domain of striatin and regulates the phosphorylation and activation of the mammalian Ste20-Like kinase Mst3.* BMC Biochem, 2011. **12**: p. 54.

73. Lu, Q., et al., *Striatin assembles a membrane signaling complex necessary for rapid, nongenomic activation of endothelial NO synthase by estrogen receptor alpha.* Proc Natl Acad Sci U S A, 2004. **101**(49): p. 17126-31.

74. Gaillard, S., et al., *Targeting of proteins of the striatin family to dendritic spines: role of the coiled-coil domain.* Traffic, 2006. **7**(1): p. 74-84.

75. Choi, Y.L., et al., *Identification of novel isoforms of the EML4-ALK transforming gene in non-small cell lung cancer.* Cancer Res, 2008. **68**(13): p. 4971-6.

76. Stephens, P.J., et al., *Massive Genomic Rearrangement Acquired in a Single Catastrophic Event during Cancer Development.* Cell, 2011. **144**(1): p. 27-40.

77. Lee, C.C., et al., *Crystal structure of the ALK (anaplastic lymphoma kinase) catalytic domain.* Biochem J, 2010. **430**(3): p. 425-37.

78. Donella-Deana, A., et al., *Unique substrate specificity of anaplastic lymphoma kinase (ALK): development of phosphoacceptor peptides for the assay of ALK activity.* Biochemistry, 2005. **44**(23): p. 8533-42.

79. Tong, Q., S. Xing, and S.M. Jhiang, *Leucine zipper-mediated dimerization is essential for the PTC1 oncogenic activity.* J Biol Chem, 1997. **272**(14): p. 9043-7.

80. Saavedra, H.I., et al., *The RAS oncogene induces genomic instability in thyroid PCCL3 cells via the MAPK pathway.* Oncogene, 2000. **19**(34): p. 3948-54.

81. Fusco, A., et al., *One- and two-step transformations of rat thyroid epithelial cells by retroviral oncogenes.* Mol Cell Biol, 1987. **7**(9): p. 3365-70.

82. Morton, C.L. and P.J. Houghton, *Establishment of human tumor xenografts in immunodeficient mice.* Nat Protoc, 2007. **2**(2): p. 247-50.

83. Yamazaki, S., et al., *Pharmacokinetic-pharmacodynamic modeling of biomarker response and tumor growth inhibition to an orally available cMet kinase inhibitor in human tumor xenograft mouse models.* Drug Metab Dispos, 2008. **36**(7): p. 1267-74.

84. Kwak, E.L., et al., *Anaplastic Lymphoma Kinase Inhibition in Non–Small-Cell Lung Cancer.* New England Journal of Medicine, 2010. **363**(18): p. 1693-1703.

85. Shaw, A.T., et al., *Crizotinib versus chemotherapy in advanced ALK-positive lung cancer.* N Engl J Med, 2013. **368**(25): p. 2385-94.

86. Doebele, R.C., et al., *Mechanisms of resistance to crizotinib in patients with ALK gene rearranged non-small cell lung cancer.* Clin Cancer Res, 2012. **18**(5): p. 1472-82.

87. Katayama, R., et al., *Two Novel ALK Mutations Mediate Acquired Resistance to the Next-Generation ALK Inhibitor Alectinib.* Clin Cancer Res, 2014.

88. Camidge, D.R., W. Pao, and L.V. Sequist, *Acquired resistance to TKIs in solid tumours: learning from lung cancer.* Nat Rev Clin Oncol, 2014. **11**(8): p. 473-81.

89. Heuckmann, J.M., et al., *ALK mutations conferring differential resistance to structurally diverse ALK inhibitors.* Clin Cancer Res, 2011. **17**(23): p. 7394-401.

90. Chen, J., C. Jiang, and S. Wang, *LDK378: a promising anaplastic lymphoma kinase (ALK) inhibitor.* J Med Chem, 2013. **56**(14): p. 5673-4.

91. Shaw, A.T. and J.A. Engelman, *Ceritinib in ALK-rearranged non-small-cell lung cancer.* N Engl J Med, 2014. **370**(26): p. 2537-9.

92. Friboulet, L., et al., *The ALK inhibitor ceritinib overcomes crizotinib resistance in non-small cell lung cancer.* Cancer Discov, 2014. **4**(6): p. 662-73.

93. Phay, J.E. and M.D. Ringel, *Metastatic mechanisms in follicular cell-derived thyroid cancer.* Endocr Relat Cancer, 2013. **20**(6): p. R307-19.

94. Frese, K.K. and D.A. Tuveson, *Maximizing mouse cancer models.* Nat Rev Cancer, 2007. **7**(9): p. 654-658.

95. Ribeiro-Neto, F., et al., *cAMP-dependent Oncogenic Action of Rap1b in the Thyroid Gland.* Journal of Biological Chemistry, 2004. **279**(45): p. 46868-46875.

96. Kim, C. and Z. Zhu, *Lessons from Mouse Models of Thyroid Cancer.* Thyroid, 2009. **19**(12): p. 1317-1331.

97. Patel, M.R., et al., *Longitudinal, Noninvasive Imaging of T-Cell Effector Function and Proliferation in Living Subjects.* Cancer Research, 2010. **70**(24): p. 10141-10149.

98. Haymart, M.R., et al., *Higher serum thyroid stimulating hormone level in thyroid nodule patients is associated with greater risks of differentiated thyroid cancer and advanced tumor stage.* J Clin Endocrinol Metab, 2008. **93**(3): p. 809-14.

99. Franco, A.T., et al., *Thyrotrophin receptor signaling dependence of Braf-induced thyroid tumor initiation in mice.* Proc Natl Acad Sci U S A, 2011. **108**(4): p. 1615-20.

100. Godbert, Y., et al., *Remarkable Response to Crizotinib in Woman With Anaplastic Lymphoma Kinase-Rearranged Anaplastic Thyroid Carcinoma.* J Clin Oncol, 2014.

101. Demeure, M.J., et al., *Whole-genome sequencing of an aggressive BRAF wild-type papillary thyroid cancer identified EML4-ALK translocation as a therapeutic target.* World J Surg, 2014. **38**(6): p. 1296-305.

102. Bhatia, P., et al., *Stem cell biology in thyroid cancer: Insights for novel therapies.* World J Stem Cells, 2014. **6**(5): p. 614-9.

103. Jung, C.W., et al., *Expression of cancer stem cell markers and epithelial-mesenchymal transition-related factors in anaplastic thyroid carcinoma.* Int J Clin Exp Pathol, 2015. **8**(1): p. 560-8.

104. Gilbertson, R.J. and T.A. Graham, *Cancer: Resolving the stem-cell debate.* Nature, 2012. **488**(7412): p. 462-3.

105. Chen, J., et al., *A restricted cell population propagates glioblastoma growth after chemotherapy*. Nature, 2012. **488**(7412): p. 522-6.

106. Zhang, W., et al., *The new concepts on overcoming drug resistance in lung cancer.* Drug Des Devel Ther, 2014. **8**: p. 735-44.

107. Katayama, R., et al., *Therapeutic strategies to overcome crizotinib resistance in non-small cell lung cancers harboring the fusion oncogene EML4-ALK.* Proc Natl Acad Sci U S A, 2011. **108**(18): p. 7535-40.

108. Katayama, R., et al., *Mechanisms of acquired crizotinib resistance in ALK-rearranged lung Cancers.* Sci Transl Med, 2012. **4**(120): p. 120ra17.

109. Lovly, C.M., et al., *Rationale for co-targeting IGF-1R and ALK in ALK fusion-positive lung cancer*. Nat Med, 2014. **20**(9): p. 1027-34.

110. Toyokawa, G., et al., *Dramatic response to crizotinib in an ALK-positive adenocarcinoma patient with disseminated intravascular coagulation.* J Thorac Oncol, 2013. **8**(11): p. e96-8.

111. Nikiforov, Y.E., et al., *Highly accurate diagnosis of cancer in thyroid nodules with follicular neoplasm/suspicious for a follicular neoplasm cytology by ThyroSeq v2 next-generation sequencing assay*. Cancer, 2014. **120**(23): p. 3627-34.

112. Nikiforova, M.N., et al., *Targeted next-generation sequencing panel (ThyroSeq) for detection of mutations in thyroid cancer.* J Clin Endocrinol Metab, 2013. **98**(11): p. E1852-60.

113. Kelly, L.M., et al., *Identification of the transforming STRN-ALK fusion as a potential therapeutic target in the aggressive forms of thyroid cancer*. Proc Natl Acad Sci U S A, 2014. **111**(11): p. 4233-8.